# MUCOSECRETORY LUNG DISEASE: DIFFERENT ASSEMBLIES OF JAG1 AND JAG2 DETERMINE TRACHEOBRONCHIAL CELL FATE

Susan D. Reynolds[1,5]

Cynthia L. Hill[1]

Alfahdah Alsudayri[1]

Scott W. Lallier[1]

Saranga Wijeratne[2]

ZhengHong Tan[3]

Tendy Chiang[3]

Estelle Cormet-Boyaka[4]

1. Center for Perinatal Research, Nationwide Children's Hospital, Columbus, OH, USA, 43215
2. Institute for Genomic Medicine, Nationwide Children's Hospital, Columbus, OH, USA, 43215
3. Center for Regenerative Medicine, Nationwide Children's Hospital, Columbus, OH, USA 43215.
4. School of Veterinary Medicine, The Ohio State University, Columbus, OH, USA, 43210
5. Contact Information: Susan D. Reynolds, PhD, Nationwide Children's Hospital, 700 Children's Drive, Columbus, OH 43205, Phone: (614) 355-6716, Fax: (614) 355-6675, Email: susan.reynolds@nationwidechildrens.org

**Word count:** 6414

**Figures:** 7

**Tables:** 0

**References:** 67

**Supplemental Information:** yes

**Running Head:** JAG1 and JAG2 determine cell fate

**Key words:** airway epithelial stem cell, Notch signaling, Jagged, cell fate, goblet cell, ciliated cell, biotinylation, ubiquitination, protein trafficking

**Author Contributions**

SDR: Conception and design, acquisition of laboratory data, interpretation of data, manuscript preparation and review.

CLH: Acquisition of laboratory data, manuscript review

AA: Acquisition of laboratory data, manuscript review

SWL: Acquisition of laboratory data, manuscript review

SW: RNAseq and scRNAseq analysis, manuscript review

ZHT: scRNAseq analysis, manuscript review

TC: Data review and interpretation, manuscript review

ECB: Data review and interpretation, manuscript review

**Funding:** Cystic Fibrosis Foundation Research Grant (REYNOL17XX0-20XX0*),* Cystic Fibrosis Foundation Therapeutics, Inc. Research Development Program Grant (MCCOY19R0), Nationwide Children's Hospital Cell Based Therapy Program (47306-0002-1217, SDR), and Nationwide Children's Hospital Technology Development Award (Technology 2019-015, SDR).

**ABSTRACT (200 WORDS):**

Mucosecretory lung disease compromises airway epithelial function and is characterized by goblet cell hyperplasia and ciliated cell hypoplasia. These cell types are derived from tracheobronchial stem/progenitor cells via a Notch dependent mechanism. Although specific arrays of Notch receptors regulate cell fate determination, the function of the ligands Jagged1 (JAG1) and Jagged2 (JAG2) is unclear. This study used primary human bronchial air-liquid-interface cultures, gamma secretase inhibition, and neutralizing antibodies to show: 1) JAG1 and JAG2 were necessary for secretory progenitor cell fate determination; 2) JAG2 suppressed squamous differentiation; and 3) pausing of the ciliated cell differentiation process after Notch inhibition. Histological, cell fractionation, cell surface biotinylation, and ubiquitination analyses demonstrated that all cells were JAG1 positive but that little JAG1 was present on the cell surface. In contrast, JAG2 was expressed in a positive-negative pattern and was abundant on the cell surface. Glycogen synthase kinase 3 (GSK3) and tankyrase inhibition studies showed that GSK3 regulated JAG2 trafficking, and that this mechanism was WNT-independent. Collectively, these data indicate that variation in JAG2 trafficking creates regions of high, medium, and low ligand expression. Thus, distinct assemblies of JAG1 and JAG2 may regulate Notch signal strength and determine the fate of tracheobronchial stem/progenitor cells.

## INTRODUCTION

The conducting airway epithelium protects the lung from inspired environmental agents via mucociliary clearance. Effective removal of pathogens, irritants, and toxins (including cigarette smoke and air pollutants) requires the coordinated activity of two specialized airway epithelial cell types, the multiciliated cell (termed a ciliated cell) and secretory cells (including goblet cells and club cells). These cell types are descendants of the tracheobronchial epithelial tissue specific stem cell (TSC) which regenerates the pseudostratified airway epithelium and resides in

68 the trachea and bronchi of the mouse and upper respiratory tract of humans. Lineage-tracing in
69 mice (1-4) and clonal analysis in human (5) indicated that the TSC was a basal cell subtype.

70 Previous studies reported that tracheobronchial ciliated and secretory cells were present in
71 approximately equal numbers and that their frequency was regulated by Notch signaling
72 (reviewed in (6)). Specifically, the Notch Lateral Induction Pathway (Notch pathway) regulates
73 basal and secretory cell differentiation (reviewed in (7)). Notch signaling occurs between
74 adjacent cells which express Notch ligands (Jagged (JAG) 1 or 2 or Delta-like (DLL) 1, 3, or 4)
75 or Notch receptors (NOTCH1, 2, 3, or 4) (6, 8). Following receptor ligation, ADAM10 or
76 ADAM17 cleaves NOTCH at an extracellular site and the γ-secretase complex cleaves NOTCH
77 at an intracellular site. This process releases the NOTCH intracellular domain which forms a
78 transcriptional complex with several proteins including RBPJK and activates expression of the
79 HES and HEY family of transcriptional repressors (9-11).

80 Chronic lung disease is frequently associated a disruption of mucociliary clearance. In asthma,
81 chronic obstructive pulmonary disease (COPD), chronic bronchitis (CB), and idiopathic
82 pulmonary fibrosis (IPF) goblet cell hyperplasia and excess mucus secretion drive the
83 mucosecretory phenotype. Single cell RNAseq (scRNAseq) analysis of asthma, IPF, and COPD
84 indicated that Notch signaling was aberrant (12-14) and functional studies indicated that
85 cigarette smoke, an agent which increases risk of developing COPD, CB, or IPF, activated
86 Notch signaling (15). Mucociliary clearance can also be disrupted by ozone and cigarette smoke
87 exposure or infection with SARS-CoV2 and/or respiratory syncytial virus. These agents damage
88 the ciliated cell, often resulting in cell death and ciliated cell hypoplasia. Notch pathway
89 components were identified as susceptibility genes for lung damage (16), viral entry (17), and
90 hyperinflammation (18). Consequently, treatments which specifically target Notch pathway
91 components have the potential to normalize ciliated and goblet cell frequency, restore
92 mucociliary clearance, and improve the health of people with chronic lung disease.

93 Several studies defined the Notch receptors responsible for generation of ciliated and secretory
94 cells in mouse and human (13, 19-23). However, the Notch ligand(s) that is responsible for
95 pathway activity is unclear. Studies in mice indicate that DLL ligands regulate generation of
96 neuroepithelial cells but are unlikely to be involved in ciliated and secretory cell differentiation
97 (24). In contrast, over-expression of *Jag2* mRNA relative to *Jag1* in basal cells (21), treatment-
98 dependent increases in *Jag1* and *Jag2* mRNA (25), and co-localization of the two mRNAs (24,
99 26) suggested overlapping roles for JAG1 and JAG2 in basal cell fate determination. Conditional
100 knockout of *Jag1* or *Jag2* early in mouse lung development supported this overlapping
101 mechanism but other studies identified JAG2 as the dominant ligand (24, 26). Finally, a specific
102 role for JAG1 in maintenance of secretory cell fate and suppression of ciliated cell fate was
103 indicated by experiments involving *Jag1* overexpression in immortalized human basal cells (27),
104 analysis of *Jag1* knockout in mice (28), and treatment of mice with a JAG1 neutralizing antibody
105 (29) or a *Jag1* antisense oligonucleotide (30).

106 A potential explanation for the disparate Jag results is the focus on the fully differentiated
107 ciliated or goblet cell. Ciliated cell subtypes have been identified by scRNAseq (31, 32), while
108 histological analysis of the mouse tracheobronchial epithelium (33) and the Xenopus epidermis
109 (reviewed in (34)) defined ciliated cell differentiation intermediates. These intermediates can be
110 detected by immunostaining for acetylated tubulin (ACT, (35)). Similarly, multiple secretory cell
111 subtypes have been identified, with the MUC5B-expressing goblet cell being the major subtype
112 (36). Goblet cell differentiation intermediates can be identified by immunostaining for MUC5B.

113 This study examined Notch signaling during differentiation of tracheobronchial TSC and
114 progenitor cells and focused on roles for JAG1 and JAG2. Cell fate determination was evaluated
115 using human bronchial air-liquid-interface cultures, a well-described and widely-utilized model of
116 the tracheobronchial epithelium (37). Treatment with γ-secretase inhibitors and analysis of
117 differentiation intermediates was used to examine Notch regulation of cell fate. Roles for JAG1

118 and JAG2 in differentiation of TSC and the secretory progenitor were evaluated using
119 histological and biochemical approaches. JAG1 and JAG2 necessity was examined using a
120 JAG1 peptide and anti-JAG1 and anti-JAG2 neutralizing antibodies.

121 **METHODS**

122 *Human TSC recovery, expansion, and ALI culture:* Human bronchial basal cells were recovered
123 as previously described (38, 39). The modified conditional reprogramming culture (mCRC)
124 method (39) was adapted from Suprynowicz et al (40). The major change from this protocol was
125 the use of irradiated NIH3T3 fibroblast feeder layers. Human basal cells were differentiated
126 using previously published methods (39). Initial studies used three culture media: Wu (41), Half
127 & Half (H&H, (35), or complete Pneumacult (Stem Cell Technology, Vancouver, BC, Canada).
128 Culture medium is defined in Results and in Figure Legends.

129 *ALI culture treatment protocol*: The specific treatment and analysis days and concentration of
130 agonists/antagonists are presented in Results and Figure Legends. Small molecule agonists
131 and antagonists were purchased from Tocris (Minneapolis, MN) and dissolved in DMSO at
132 1000x the treatment concentration. Vehicle controls were treated with an equal volume of
133 DMSO. Jag1 peptide was purchased from Anaspec (Freemont, CA) and dissolved in 1x
134 Phosphate Buffered Saline (PBS) at 500x the treatment concentration. Vehicle controls were
135 treated with an equal volume of PBS. Neutralizing antibodies specific for Jag1 (anti-JAG1.b70)
136 and Jag2 (anti-JAG2.b33) were provided by Genentech (29) and were dissolved in PBS at 100x
137 the treatment concentration. Vehicle controls were treated with an equivalent volume of PBS.

138 *Immunofluorescence analysis and quantification*: Differentiation was evaluated in ALI cultures.
139 Cultures were fix with 4% paraformaldehyde/1% sucrose/1x PBS. For analysis of intracellular
140 markers cultures were permeabilized and blocked with 0.1% NP40/5% bovine serum albumin/1x
141 PBS. For analysis of cell surface markers, cultures were fixed with 10% neutral buffered
142 formalin and blocked with 5% bovine serum albumin/1x PBS. Goblet cells and differentiation

143 intermediates were identified by MUC5B staining using rabbit-anti-MUC5B (Sigma, 1/500).
144 Ciliated cells and differentiation intermediates were identified by ACT staining using mouse-anti-
145 ACT (Sigma, 1/8000). JAG1 was evaluated using a mouse-anti-JAG1 C-terminal specific
146 antibody (BD Biosciences #612346, 1/50). JAG2 was evaluated using a rabbit-anti-JAG2 N-
147 terminal specific antibody (Cell Signaling C23D2, 1/50) and a rabbit-anti-JAG2 C-terminal
148 specific antibody (Cell Signaling C83A8, 1/50). HES1 was evaluated using a goat-anti-HES1
149 (Santa Cruz #sc-13842, 1/40). Rbpjk was evaluated using a rabbit-anti-RBPJK (Sigma
150 #AB5790, 1/100). Primary antibodies were detected with ALEXA-488 or ALEXA-594 labeled
151 secondary antibodies (Jackson Immunological, 1/500). Nuclei were detected with DAPI. Cell
152 type frequency was quantified as previously described (39).

153 *Cell fractionation:* Cells were separated into cytoplasmic and nuclear fractions using a NE-PER
154 kit (Thermo Scientific, P178833). 4x Laemmli's Buffer/10% β-mercaptoethanol (BME) was
155 diluted 1/4 into the protein fraction and the mixture was incubated at 96 ˚C for 10 minutes.

156 *Cell lysis:* RIPA buffer (42) was used to lyse cells for immunoprecipitation, poly-ubiquitination,
157 and western blot analysis. The apical and basal surfaces of ALI cultures were washed with
158 Hams/F12 at 4 ˚C for 10 min. Wash solution was aspirated and 270 µl RIPA buffer was added to
159 the apical surface. The cell layer was disrupted with a p200 pipette tip and then incubated for 20
160 min at 4 ˚C. The lysate was collected in a 1 ml microcentrifuge tube, sonicated 5 x 30 sec in a
161 Bioruptor (Diagenode) at 4 ˚C, and centrifuged at 11,176g for 10 min at 4 ˚C. The supernatant
162 was stored at -80 ˚C.

163 *Immunoprecipitation:* Immunoprecipitation was performed using a modified version of the Pierce
164 Protein Magnetic Bead protocol (Thermo 88848). For each sample, 125 µl of beads were pre-
165 washed three times with RIPA Buffer and resuspended in RIPA Buffer with proteinase (Roche;
166 11836153001) and phosphatase inhibitors (Roche; 04906837001). Washed beads (25 µl) were
167 added to 400-600 ug protein per sample and the lysate was cleared by rocking for 1 hr at 4 ˚C.

168 The cleared lysate was incubated with a titration-determined amount of antibody (usually 1:100).
169 This mixture was rocked for 1 hr at 4 ˚C. The remaining 100 µl of washed beads were added to
170 the sample and rocked for 2 hr at 4 ˚C. The beads were collected using a neodymium magnet,
171 washed three times with RIPA Buffer, resuspended in 1x Laemmli's Buffer plus 2.5% BME, and
172 incubated at 96 ˚C for 10 minutes. The supernatant was kept as Unbound Fraction.

173 *Cell surface biotinylation:* A modified version of the Pierce Cell Surface Protein Biotinylation and
174 Isolation Kit (Thermo A44390) protocol was used to isolate surface proteins. The recommended
175 biotinylation incubation time was increased to 45 minutes and incubations were done on ice.

176 *Poly-ubiquitination:* Total Poly-ubiquitinated proteins were isolated using a LifeSensors Tandem
177 Ubiquitin Binding Entities (TUBEs) Kit (LifeSensors, UM411M) and a modified protocol. The cell
178 lysate was incubated with 100 µl washed, unconjugated beads at 4 ˚C on a rotating platform for
179 30 minutes. A bead titration study demonstrated an optimal ratio of 100 µl TUBE-conjugated
180 beads per 1-2 mg protein in a total of 1 ml lysis buffer. The cleared lysate and washed TUBE
181 beads were incubated at 4 ˚C on a rotating platform for 30 minutes. The TUBE beads were
182 collected using a magnet, washed three times with PBST, and divided into two aliquots. One
183 aliquot was treated with buffer and the second aliquot was treated with 2 µl of 10 µM broad-
184 spectrum deubiquitinase for 2hr at 30˚C with rocking. The beads were resuspended in 1x
185 Laemmli's Buffer/2.5% BME and incubated for 10 minutes.

186 *Western blot analysis and quantification*: Protein concentration, gel electrophoresis and transfer,
187 and blotting were done as previously reported (42). In some instances, blots were stripped by
188 incubation with 1X Western Reprobe (G Biosciences) for 45 minutes at 55 ˚C followed by three
189 washes with Tris buffered saline with TWEEN-20 (TBS-T, Cell Signaling Technology) at room
190 temperature. Antibodies used for western blot studies: JAG2-N-terminal (Cell Signaling C23D2,
191 1:1000); JAG2-C-terminal (Cell Signaling C83A8, 1:1000); GSK3 (Millipore 05-412, 1:2000);
192 pGSK3 (Millipore 0-413, 1:1000); 14-3-3 (Millipore AB9748-I, 1:2000); TOPO II (Abcam 109524,

193 1:10000); Sodium Potassium ATPase (NAK, Cell Signaling 3010S, 1:2500); JAG1-C-terminal
194 (BD Biosciences #612346, 1:1000); α-Tubulin (Sigma T6793, 1:2000); N-terminal β-catenin Cell
195 Signaling #9581X, 1:1000); C-terminal β-catenin (BD Transduction #610154, 1:2000); and
196 Keratin 5 (BioLegend #905501, 1:2000).

197 *RNA preparation and RNAseq gene expression analysis:* RNA was purified using a RNeasy Kit
198 (Qiagen,74106) according to the manufacturer's directions. RNA-sequencing (RNAseq) was
199 conducted by the Institute for Genomic Medicine at Nationwide Children's Hospital. On average,
200 32 million paired-end 151 bp RNA-Seq reads were generated for each sample (the range was
201 25 to 37 million). Each sample was aligned to the GRCh38.p9 assembly of the Human
202 reference from NCBI (http://www.ncbi.nlm.nih.gov/assembly/GCF_000001405.35/) using
203 version 2.6.0c of the RNA-Seq aligner STAR
204 (http://bioinformatics.oxfordjournals.org/content/29/1/15). Transcript features were identified
205 from the GFF file provided with the assembly from Gencode (v28) and raw coverage counts
206 were calculated using featureCounts (http://bioinf.wehi.edu.au/featureCounts/). The raw RNA-
207 Seq gene expression data was normalized and post-alignment statistical analyses were
208 performed using DESeq2 (http://genomebiology.com/2014/15/12/550) and custom analysis
209 scripts written in R. Comparisons of gene expression and associated statistical analysis were
210 made between different conditions of interest using the normalized read counts. All fold change
211 values are expressed as test condition / control condition, where values less than one are
212 denoted as the negative of its inverse (note that there will be no fold change values between –1
213 and 1, and that the fold changes of "1" and "-1" represent the same value). Transcripts were
214 considered significantly differentially expressed using a 10% false discovery rate (DESeq2
215 adjusted p value <= 0.1). GSEA was used to identify treatment dependent changes in signaling.

216 *scRNAseq data analysis*: Single cell RNAseq methods and analytical techniques are presented
217 in detail in (13) and (43). The raw reads were processed with Cell Ranger software 3.0.2 (10X

218 Genomics) using hg38 transcriptome reference from GENCODE 25 annotation, and a digital
219 expression matrix was generated with cell barcodes as rows and gene identities as columns.
220 Each dataset was run with SoupX analysis package to remove contaminant 'ambient' RNA
221 derived from lysed cells during isolation and capture (44). To minimize doublet contamination,
222 for each dataset the Scrublet package was used to detect neotypic doublets (45) and a quantile
223 thresholding was performed to identify high UMI using a fit model generated using multiplet's
224 rate to recovered cells proportion, as previously described (43). For all data, quality control and
225 filtering were performed to remove cells with low number of expressed genes (threshold
226 n>=200) and elevated expression of apoptotic transcripts (threshold mitochondrial genes <
227 15%). Only genes detected in at least 3 cells were included. Data were normalized using the
228 Scran package (46), using a low resolution clustering to use as input for the size factor
229 estimation and then log transformed. Data were processed with Principal Component Analysis
230 (PCA) using the 5000 most variable genes as input, and clustering was performed with the
231 Leiden algorithm. Batch correction for the two samples was performed with the package BBKNN
232 (Polanski et al., 2019). Partition-based graph abstraction (PAGA) (47) was added to Uniform
233 Manifold Approximation and Projection (UMAP) with the option init_pos='paga' (48) to obtain a
234 two-dimensional visualization. To identify differentially expressed genes between clusters and
235 representative of both datasets, Model-based Analysis of Single-cell Transcriptomics (MAST)
236 (49) was used. To characterize cell subsets in our integrated dataset, previously published lung
237 cell subtype specific gene lists (43) were used to create cell type-specific gene signatures using
238 a strategy previously described (50). The steps described above were generated using Seurat
239 3.0 in R 4.0 or Scanpy 1.7.0 in Python 3.8.5. Plots were generated within Seurat and Scanpy or
240 using the ggplot2 package.

241 *Statistics*: All statistical analyses were performed using Graph Pad Prism. Data normality was
242 evaluated by the Shapiro-Wilk test, the Anderson-Darling test, and/or the D'Agostino & Pearson

243 test. For normally distributed data sets, differences were evaluated using Student's t-test. For
244 non-normally distributed data sets, differences were evaluated by the Mann-Whitney test and
245 data are presented as the median and the interquartile range. Trends were analyzed by
246 regression analysis. The definition of center and dispersion precision measures are indicated in
247 the Figure Legends. Data sets containing multiple variables were analyzed by analysis of
248 variance (ANOVA) and a post hoc Tukey test (normally distributed data sets) or Kruskal Willis
249 test (non-normally distributed data sets). Sample size is indicated in the Figure Legends. P-
250 values < 0.05 were considered significant.

251 *Study approval:* The Institutional Review Board at Nationwide Children's Hospital approved the
252 human studies. Written informed consent and assent was obtained from every participant.

253 **RESULTS**

254 *Ciliated and goblet cell differentiation*: Since kinetics and cell type frequency vary across model
255 systems, differentiation was evaluated in three differentiation media. Quantification
256 demonstrated that cell density did not vary as a function of medium or time (SFig 1A) and that
257 the frequency of ciliated cells increased significantly between differentiation days 7 and 14 in all
258 three media (SFig 1B). The frequency of mature goblet cells did not vary between differentiation
259 days 7 and 14 in Wu or complete Pneumacult medium but increased significantly in Half&Half
260 (H&H) medium (SFig 1C). Based on the finding that H&H medium supported an increase in
261 ciliated and goblet cell frequency over days 7-14 and generated similar numbers of goblet and
262 ciliated cells on day 14, this medium was used to evaluate the signaling mechanisms that
263 regulate production of ciliated and goblet cells.

264 *Intermediate ciliated and goblet cell phenotypes*: Previous work demonstrated that ciliated cell
265 differentiation involved a set of intermediate phenotypes (reviewed in (34)). In Stage I, cells exit
266 the cell cycle and express a primary cilium (SFig 2A-B). This phenotype was detected at early
267 time points and the frequency of cells with a primary cilium peaked on differentiation day 6 (Fig

268 1A). During Stages II and III, new centrioles are generated and dock at the apical cell surface.
269 Cells that contained many basal bodies and occasional short cilia (bristle cells, SFig 2C-D) were
270 identified on days 8-12 (Fig 1B). Finally, during Stage IV, each docked centriole (now termed a
271 basal body) nucleates a motile 9+2 ciliary axoneme and the ciliary appendage is formed. Cells
272 defined many long motile cilia (ciliated cells, SFig 2E-F) were detected on days 8-12 (Fig 1C).

273 Goblet cells also exhibited three morphological phenotypes that were defined by low, medium,
274 and high expression of MUC5B (SFig 2G-H). All three intermediates were detected at all time
275 points (Fig 1D-F). The frequency of MUC5B-low and MUC5B-medium cells peaked on day 8
276 while the frequency of MUC5B-high cells increased through day 12 (Fig 2F). These data
277 indicated that the first wave of ciliated and goblet cell differentiation was completed the process
278 by day 12.

279 *Notch regulation of ciliated and goblet cell differentiation*: Previous studies demonstrated that
280 treatment with DAPT, a γ-secretase inhibitor (GSI), inhibited Notch signaling, increased the
281 frequency of ciliated cells, and decreased the frequency of mature goblet cells (35). To
282 determine if this paradigm applied to the first wave of differentiation, H&H cultures were treated
283 with DAPT on days 0-4, 2-6, 4-8, or 8-12. DAPT treatment did not alter cell density at any time
284 point (SFig 3).

285 DAPT treatment significantly increased the frequency of cells with a primary cilium on day 4 (Fig
286 1A), significantly increased the frequency of bristle cells on days 4, 6, and 8 (Fig 1B), and
287 significantly increased the frequency of ciliated cells on days 8 and 12 (Fig 1C). DAPT treatment
288 did not alter the frequency of MUC5B-low or MUC5B-medium cells at any time point (Fig 1D-E).
289 However, DAPT treatment significantly decreased the frequency of MUC5B-high cells on days 8
290 and 12 (Fig 1F). Similar results were gathered in experiments using a second GSI, LY411575
291 (LY, data not shown). Collectively, these data indicated that Notch signaling was active during
292 the first wave of differentiation.

293 *Pausing of the Notch signal:* Accumulation of ciliated cell differentiation intermediates suggested
294 that GSI treatment paused the ciliation process. To investigate this mechanism, cultures were
295 treated with LY for 4 days and recovered (recovery) or treated with LY for 8 days (continuous,
296 Fig 2A). On differentiation day 12, ciliated and goblet cell intermediates were quantified. Cells
297 with a primary cilium were not detected in these cultures (Fig 2B). Both bristle and ciliated cells
298 were detected, and their frequency did not vary between the recovery and continuous treatment
299 protocols (Fig 2B). Goblet cells defined by low, medium, and high expression of MUC5B were
300 identified but their frequency did not vary with treatment. Since continuous Ly treatment did not
301 cause an increase in bristle or ciliated cell frequency, these data indicated that GSI treatment
302 paused ciliated cell differentiation.

303 Since Notch signaling in the tracheobronchial epithelium has been attributed to JAG1 and
304 JAG2, the impact of GSI treatment on JAG1 or JAG2 protein abundance was determined.
305 Cultures were treated with LY or DAPT on days 4 and 6 and protein expression was analyzed
306 by western blot on day 8. GSI treatment did not alter JAG1 abundance (Fig 2C). In contrast, GSI
307 treatment significantly increased the abundance of full-length JAG2 (Fig 2D). These data
308 suggested that GSI treatment paused the differentiation process by increasing JAG2.

309 *Cellular localization of JAG1 and JAG2*: A JAG2-dependent pausing mechanism was
310 unanticipated and supported an in-depth analysis of JAG1 and JAG2 distribution on
311 differentiation day 7. Immunofluorescence analysis detected JAG1 in cultures that were
312 differentiating in each test medium (SFig 4A-C, 4J-K) and showed that JAG1 was highly
313 localized to the perinuclear/nuclear compartments. All cells were positive for JAG1. JAG2 was
314 also detected in all three culture conditions but was most abundant in cultures that were
315 differentiating in H&H medium (SFig 4D-F, 4J-K). In contrast with JAG1, JAG2 was highly
316 enriched in the cortical domain. All cells were positive for JAG2; however, expression varied
317 from low to high.

318 *JAG1 subcellular location and molecular weight*: The subcellular location of JAG1 on
319 differentiation day 7 was unexpected and led to analysis at additional time points. On
320 proliferation day 3 (Fig 3A, D, E) and differentiation day 2 (Fig 3B), JAG1 was expressed in a
321 subset of cells and was in the perinuclear/nuclear domain. JAG1 did not colocalize with β-
322 catenin, a component of the adherens junction (Fig 3F-G). On differentiation day 4 (Fig 3C),
323 JAG1 was detected in most cells and some variation in protein abundance was noted.

324 Previous studies reported that Notch ligands can be cleaved by γ-secretase resulting in creation
325 of a transcriptionally active 25 kDa C-terminal peptide (51-53). Consequently, JAG1 molecular
326 weight was determined using a JAG1 antibody which detected the C-terminal domain. On days
327 4 and 8, all samples contained the full-length (~130 KDa) JAG1 protein (Fig 3H). To further
328 examine JAG1 subcellular localization, cytoplasmic and nuclear fractions were isolated on day
329 8. Detection of Topoisomerase II in the nuclear fraction and alpha tubulin in the cytoplasmic
330 fraction (Fig 3I) demonstrated successful separation. JAG1 was limited to the cytoplasmic
331 fraction and indicated that the protein was perinuclear rather than nuclear.

332 Since the previous studies indicated that most if not all JAG1 was in a perinuclear compartment
333 and that JAG1 was not acting as transcription factor, the relationship between transcription and
334 translation was evaluated. *Jag1* mRNA was quantified by RNAseq and JAG1 protein levels
335 were quantified by Western blot. *Jag1* abundance decreased as a function of time (Fig 3J). In
336 contrast, JAG1 abundance was constant over time (Fig 3K). These data suggested that a post-
337 translational mechanism regulated JAG1 abundance.

338 *JAG2 subcellular location and molecular weight*: JAG2 localization was further evaluated on
339 proliferation day 5 and differentiation days 4 and 8 (Fig 4A-C). The cortical pattern was
340 observed on proliferation day 5 and JAG2-high cells were apparent on differentiation day 4. By
341 differentiation day 8, JAG2-positive and -negative cells were noted. At each time point, JAG2

342 colocalized with β-catenin. On differentiation day 8, groups of cells expressing nuclear HES1
343 and RBPJK were detected (Fig 4D) and indicated focal Notch signaling.

344 The molecular weight of JAG2 was determined using two antibodies which were specific to the
345 N-terminal or C-terminal domains. This study detected full-length (~145 KDa) JAG2 on days 4
346 and 8 (Fig 4E). To further examine JAG2 subcellular localization, co-immunoprecipitation was
347 used to determine if JAG2 was associated with the adherens junction. An N-terminal specific β-
348 catenin antibody was used for immunoprecipitation and the precipitate was analyzed with N-
349 terminal and C-terminal specific β-catenin antibodies. β-catenin was successfully isolated (Fig
350 4F) and JAG2 was identified in the β-catenin complex.

351 Since the previous studies suggested that much of JAG2 was trafficking to or from the plasma
352 membrane, the relationship between transcription and translation was evaluated using RNAseq
353 and western blots. *Jag2* abundance decreased as a function of time (Fig 4G). In contrast, JAG2
354 abundance was constant over time (Fig 4H). Like JAG1, these data suggested a post-
355 translational mechanism regulated JAG2 abundance.

356 *Regulation of JAG2 abundance*: Identification of JAG2-positive and JAG2-negative cells on
357 differentiation day 8 suggested that JAG2 was degraded in some cells. A candidate regulator is
358 the WNT/β-catenin pathway (35). To examine this mechanism, ALI cultures were treated with
359 various concentrations of CHIR99021 (CHIR, a WNT/β-catenin agonist, (54)) or XAV939 (XAV,
360 a WNT/β-catenin antagonist, (55)) on differentiation days 4 and 6 and cell lysates were collected
361 on day 8. Western blot analysis demonstrated that neither CHIR nor XAV treatment altered the
362 abundance of JAG1 (Fig 5A). In contrast, both treatments caused a significant decrease in
363 JAG2 abundance (Fig 5B). Interestingly, the CHIR effect was limited to lower doses (5 and 10
364 μM); whereas the XAV effect was observed at all three doses.

365 *Impact of CHIR and XAV on the transcriptome:* CHIR and XAV are typically thought to regulate
366 WNT/β-catenin pathway by altering gene expression. To evaluate this mechanism, ALI cultures

367 were treated with vehicle, 10 μM CHIR or 10 μM XAV on differentiation days 4 and 6 and RNA
368 was purified on day 8. RNA-sequencing and Gene Set Expression Analysis (GSEA)
369 demonstrated that CHIR upregulated expression of WNT/β-catenin target genes including
370 *Axin2*, *Lef1*, *Tcf7* (SFig 5A-B, SFig 6). These genes contributed to the GSEA Leading-Edge and
371 had a high impact on the GSEA Enrichment Score (an indicator of changes in pathway activity).
372 Other GSEA Leading-Edge genes were *Wnt5B* and known pathway antagonists (*Axin1, Dkk1*,
373 *Dkk4,* and *Nkd1*). Since these genes and *Axin2* inhibit the WNT/β-catenin pathway and *Lef1*
374 and *Tcf7* repress gene expression, these data suggested that CHIR antagonized the WNT/β-
375 catenin pathway on day 8.

376 In keeping with its perceived function as a WNT/β-catenin pathway antagonist, XAV treatment
377 downregulated expression of *Axin2*, *Lef1*, and *Tcf7*, and *Wnt5B* (SFig 5C-D, SFig 6). However,
378 most GSEA Leading-Edge WNT/β-catenin pathway genes were typical of the Notch pathway
379 (*Dll1*, *Hey1*, *Jag1*, *Jag2*, *Notch1*, and *Notch4*). Analysis of the Notch gene set indicated that
380 XAV treatment caused a significant downregulation of Notch signaling (SFig 5G-H). A similar
381 analysis of the Notch gene set in CHIR treated cultures also indicated downregulation (SFig 5E-
382 F). Although the high FDR q-value suggested cautious interpretation of the CHIR-Notch
383 pathway interaction, many of the GSEA Leading-Edge genes were shared between the CHIR
384 and XAV groups (*Dll1*, *Jag1*, *Notch1*, *Lfng*, *Prkca*, *Psenen*, *Sap30*, and St3gal6, SFig 5E-H,
385 SFig 6).

386 Although *Jag1* and *Jag2* contributed to the Enrichment Scores, neither gene product was
387 consistently included in the GSEA Leading-Edge gene sets. Consequently, the impact of CHIR
388 and XAV treatment on gene expression was evaluated. *Jag1* and *Jag2* abundance did not vary
389 by treatment (SFig 5I-J). Collectively, the gene expression data indicated that the main effect of
390 CHIR or XAV treatment was to antagonize WNT/β-catenin and Notch signaling and that
391 decreased signaling could not be attributed to a change in *Jag1* or *Jag2* gene expression.

392 *WNT independent regulation of JAG2 abundance*: To examine the impact of WNT antagonism
393 on JAG1 and JAG2 abundance, ALI cultures were treated with vehicle, LGK974 (LGK) a
394 porcupine inhibitor which prevents WNT secretion, or DKK1 which inhibits WNT signaling by
395 binding the LRP5/6 coreceptor. Neither LGK treatment (Fig 5A-B) nor DKK1 treatment (Fig 5C-
396 D) altered JAG1 or JAG2 abundance. These data suggested that a WNT-independent
397 mechanism regulated the abundance of JAG2 in CHIR and XAV treated cultures.

398 *CHIR regulation of cell fate*: While the decrease in JAG2 abundance in response to CHIR or
399 XAV treatment was unexpected, a previous study reported that both drugs altered secretory and
400 ciliated cell differentiation (35). To further examine changes in cell fate, ALI cultures were
401 treated with CHIR on days 4 and 6 and cells were isolated for single cell RNAseq in day 8.
402 Fourteen clusters (0-13) were identified (Fig 5E, F) and 10 clusters differed significantly
403 between vehicle and CHIR treated cultures (Fig 5G). In vehicle treated controls, clusters 6, 8,
404 and 10 exhibited a mitotic signature (STable 1). The frequency of cells in these clusters
405 increased in CHIR treated cultures. Cluster 1 was prominent in vehicle treated cultures and
406 contained basal cells which exhibited a matrix production signature. This cluster over-expressed
407 *Jag2* and *Wnt4* and was nearly absent in CHIR treated cultures. Clusters 4, 0, 3 and 12
408 contained cells within the secretory lineage and clusters 4, 0 and 3 expressed Hes4, Hes1,
409 and/or Hes2. Cluster 3 contained secretory primed basal cells that were defined by expression
410 of *Ceacam6*, *Scgb1A1*, and *Scgb3A2*. Cells within cluster 3 were less mature than those in
411 cluster 12. Clusters 4, 0 and 3 were significantly decreased in CHIR treated cultures. Clusters
412 13 and 5 contained ciliated cell lineage cells. Cluster 13 was enriched in early-stage ciliated
413 cells defined by expression of *Mcidas* and cluster 5 contained more mature ciliated cells. Cluster
414 2 was increased in CHIR treated cultures and clusters 7 and 9 were unique to CHIR treated
415 cultures. Cluster 7 was distinguished by down-regulation of WNT pathway antagonists (*Axin2*,
416 *Dkk2*, *Dkk4*, *Nkd1*), and the presence of cell motility and keratinization signatures. The

417 keratinization signature was upregulated in clusters 2 and 9. Since keratinization was previously
418 associated with squamous differentiation in the tracheobronchial epithelium (56), these data
419 indicated that CHIR treatment promoted this fate and suggested that JAG2 suppressed
420 squamous differentiation.

421 *JAG1 and JAG2 trafficking to the cell surface*: To further investigate roles for JAG1 and JAG2 in
422 Notch signaling, cell surface protein was evaluated by immunofluorescence analysis of non-
423 permeabilized cultures. JAG1 was not detected on the cell surface on differentiation day 8. In
424 contrast, JAG2 was detected on the surface of many cells (Fig 6A-B). Subsequent
425 permeabilization and staining detected both JAG1 and JAG2 and illustrated their typical
426 intracellular distributions (Fig 6C-F).

427 Cell surface biotinylation was used to evaluate JAG1 and JAG2 trafficking to the plasma
428 membrane. These studies detected sodium/potassium ATPase (NKA) a known cell surface
429 protein as well as JAG1 and JAG2 (Fig 6G). However, cell surface JAG2 was 5-10 times more
430 abundant than JAG1. Since interaction with a Notch receptor results in ligand ubiquitination and
431 internalization, polyubiquitination of JAG1 and JAG2 was analyzed. Little or no JAG1 was
432 detected in the bound (ubiquitin-positive) fraction (Fig 6H, upper panel). In contrast, JAG2 was
433 detected in the bound fraction and the molecular weight of the captured JAG2 decreased after
434 treatment with a deubiquitinase (Fig 6H). These biochemical studies indicated that JAG2
435 participated in Notch-signaling and raised the possibility that JAG1 was not involved.

436 *Phosphorylation of JAG2*: Immunofluorescence analysis demonstrated that CHIR treatment
437 caused a striking redistribution of JAG2 to a perinuclear location (Fig 6I-J) and was suggestive
438 of JAG2 degradation. JAG2 was not detected by immunofluorescence staining in XAV treated
439 cells (data not shown). CHIR is a potent and highly selective inhibitor of GSK3 (54). In contrast,
440 XAV inhibits tankyrase and regulates GSK3 by altering the kinase's localization within the cell
441 (55). Since both drugs decrease GSK3 activity and decrease JAG2 abundance, it was possible

442 that the shared mechanism was a GSK3-dependent decrease in JAG2 phosphorylation. To
443 evaluate this mechanism, differentiation day 8 cell lysates were immunoprecipitated with an
444 anti-pSerine/pThreonine (pS/pT) antibody and western blots were probed for JAG2 and positive
445 controls (KRT5 and YWHA). This study detected JAG2, KRT5 and YWHA in the bound fraction
446 (Fig 6K) and indicated that JAG2 was phosphorylated on Serine and/or Threonine. Collectively,
447 these data suggested that normal JAG2 trafficking was dependent on phosphorylation by GSK3.

448 *Roles for JAG1 and JAG2 in Notch Signaling*: To determine if JAG1 was involved in Notch
449 signaling, cultures were treated with a JAG1 DSL-domain peptide on differentiation days 8 and
450 10 and cultures were fixed on differentiation day 12. Immunofluorescence analysis of ACT and
451 MUC5B was used to detect differentiation intermediates. Cells expressing a primary cilium were
452 not detected (Fig 7A). However, vehicle treated cultures contained a small number of bristle
453 cells and many ciliated cells. Treatment with the JAG1 peptide caused a significant increase in
454 the frequency of bristle cells but did not alter the frequency of ciliated cells (Fig 7A). The same
455 cultures did not contain MUC5B-low cells (Fig 7B). However, MUC5B-medium, and MUC5B-
456 high cells were detected. Treatment with JAG1 peptide did not alter the frequency of MUC5B-
457 medium cells but significantly decreased the frequency of MUC5B-high cells. These data
458 suggested two JAG1-dependent processes. First, that the JAG1 peptide inhibited Notch
459 signaling resulting in increased basal-to-bristle cell differentiation. Second, the decreased
460 maturation of MUC5B-medium cells combined with the increase in bristle cell frequency raised
461 the possibility that JAG1 peptide treatment promoted MUC5B-medium to ciliated cell
462 differentiation.

463 Since the JAG1 peptide is 71% identical to the JAG2-DSL domain, it was unclear if the JAG1
464 peptide results could be attributed to JAG1. Further, the JAG1 peptide results were consistent
465 with reports that used JAG1 peptide to antagonize Notch signaling (57) but disagreed with those

466 reporting that this reagent agonized Notch signaling (58, 59). Consequently, additional studies
467 used neutralizing antibodies to inhibit JAG1 or JAG2 activation of Notch receptors (29).

468 To address the limitations of the JAG1 peptide studies, ALI cultures were treated with
469 neutralizing antibodies on days 8 and 10 and ciliated and secretory cell differentiation was
470 assayed on day 12. Treatment with anti-JAG1 or anti-JAG2 significantly increased bristle cell
471 frequency and decreased ciliated cell frequency (Fig 7C-D). Neutralizing antibody treatment did
472 not alter the frequency of MUC5B-medium cells but significantly decreased the frequency
473 MUC5B-high cells (Fig 7E-F). These data suggested that loss of either JAG1 or JAG2 caused
474 MUC5B-medium cells to generate bristle cells. To address the finding that anti-JAG1 or anti-
475 JAG2 treatment decreased ciliated cell frequency, ALI cultures were treated with a mixture of
476 anti-JAG1 and anti-JAG2. This treatment significantly decreased bristle cell frequency but did
477 not alter ciliated cell frequency (Fig 7G-H). The combined neutralizing antibody treatment did
478 not alter the frequency of MUC5B medium cells and significantly decreased the frequency of
479 MUC5B-high cells (Fig 7I-J). These data in combination with the single antibody study indicated
480 that either JAG1 or JAG2 inhibited bristle cell to ciliated cell differentiation.

481 **DISCUSSION**

482 This study demonstrated that JAG1 and JAG2 cooperate to determine the fate of the MUC5B-
483 medium (secretory progenitor) cell (SFig 7A). The neutralizing antibody studies found that both
484 JAG1 and JAG2 were required to generate a mature MUC5B-high goblet cell. In contrast,
485 neutralization of either JAG1 or JAG2 allowed the MUC5B-medium cell to generate a bristle cell.
486 Finally, the CHIR and XAV studies indicated that degradation of JAG2 resulted in a squamous
487 fate (SFig 7B). While these data support the paradigm that high Notch signal strength selected
488 the goblet cell fate, the possibility of moderate and low Notch intensity within the secretory
489 lineage was novel.

490 Previous studies indicated that cell fate was determined by different assemblies of Notch
491 receptors (13, 20). The present study suggests that different assemblies of JAG ligands
492 determine Notch signal intensity. First, JAG1 was detected in all differentiating cells. Second, a
493 striking change in cell morphology coincided with the emergence of JAG2 positive and negative
494 cells and raised the possibility that increased polarization concentrated JAG2 at cell-cell
495 junctions (60). When combined with the histological and biochemical data, these studies
496 indicated that JAG1 might establish a minimum ligand concentration while changes JAG2
497 trafficking result in cells that express high or low levels of cell surface ligand. Thus, it is possible
498 that the MUC5B-medium cell fate is determined by its location in a ligand-low (JAG1 only),
499 ligand-medium (mixture of JAG1+/JAG2+ and JAG1+/JAG2- cells), or a ligand-high
500 (JAG1+/JAG2+) environment (Graphical Abstract).

501 This study also indicated that JAG2 paused the ciliated cell differentiation process (SFig 7C).
502 Initial support for pausing came from the finding that GSI treatment increased the frequency of
503 ciliated cell differentiation intermediates. These data suggested that Notch signaling fluctuated
504 from “off” to “on” as the cell progressed from one morphological intermediate to the next. These
505 data challenged the idea that ciliated differentiation occurred in the absence of a Notch signal
506 but also raised the possibility that the GSI-sensitive target was the ligand rather than the
507 receptor. Support for the latter idea comes from previous demonstration that JAG1 and JAG2
508 were cleaved by γ-secretase resulting in production of an intracellular domain which functions
509 as a transcription factor (51-53). Failure to detect the ~25 kDa intracellular domain may reflect
510 low sensitivity in the ALI model relative to ligand over-expression systems.

511 Evidence of pausing also challenged the notion that ciliated cell differentiation was continuous
512 and suggested that differentiation occurred in incremental steps. Demonstration that expression
513 of a ciliated transcription network gene product, *cMyb,* fluctuated over time and regulated
514 progression through the ciliated cell differentiation program (61) supported this interpretation.

515 Although the neutralizing antibody studies indicated that bristle-to-ciliated cell differentiation
516 occurred only when JAG1 and JAG2 were blocked, western blot analysis correlated the GSI-
517 dependent signal with an increase in full-length JAG2 abundance. Since gene expression
518 studies indicated that GSI treatment did not alter *Jag2* (or *Jag1*) mRNA abundance, it is
519 possible that pausing involved a change in JAG2 protein trafficking.

520 Previous studies showed that transmembrane proteins, including JAG1 and JAG2, transit the
521 endocytic recycling compartment as they move to the plasma membrane. This compartment is
522 positioned under the nucleus in adherent cells, and sorts endocytosed proteins that are recycled
523 to the plasma membrane, enter the lysosome for degradation, or are sequestered in a
524 perinuclear site termed the pericentrion (62). A protein's trafficking pattern is determined in part
525 by phosphorylation and ubiquitination and changes in the rate of movement through the various
526 endosomal compartments regulate Notch signaling (63).

527 This study identified a striking difference in JAG1 and JAG2 localization within the cytoplasm of
528 differentiating cells. Cell fractionation studies indicated that JAG1 was highly enriched in the
529 perinuclear domain. Demonstration that JAG1 was not poly-ubiquitinated indicated that most
530 JAG1 was in the endocytic recycling compartment and not sequestered in the pericentrion. In
531 contrast, the subcellular distribution and polyubiquitination of JAG2 were consistent with
532 endocytosis, recycling through the endocytic pathway, and post-signaling degradation via the
533 lysosome. Increased JAG2 protein levels in GSI-treated cultures and decreased JAG2 levels in
534 CHIR and XAV treated cultures suggested that JAG2 routing could be altered and that JAG2
535 and GSK3 might be co-localized in multivesicular bodies (64, 65).

536 A previous study reported that NOTCH1 trafficking to the cell surface was inhibited by GSK3-
537 mediated phosphorylation (66) while the present study showed that GSK3 inhibition resulted in
538 JAG2 degradation. Consequently, GSK3 activity might determine if a cell traffics JAG2 or
539 NOTCH1 to the cell surface. Although the WNT/β-catenin pathway was a likely regulator of

540 GSK3 activity, our previous report found that CHIR and XAV (35) inhibited ciliated cell and
541 goblet cell commitment and suggested a complex mechanism. The present study indicates that
542 both CHIR and XAV antagonized WNT/β-catenin signaling and that the main effect of these
543 drugs was downregulation of Notch signaling. Although these data suggest that Notch signaling
544 is dependent on β-catenin, a role for WNT signaling was discounted by studies which inhibited
545 WNT secretion or WNT interaction with LRP6/5. A similar WNT ligand-independent role for
546 GSK3 in cell fate specification was previously reported for iPSC that were undergoing directed
547 differentiation (67) and suggested that establishment of tracheobronchial ligand- and receptor-
548 expressing cells was regulated by a GSK3-dependent and WNT-independent mechanism.

549 **CONCLUSION**

550 This study demonstrates that JAG1 and JAG2 are necessary for cell fate specification within the
551 tracheobronchial epithelium. Differences in JAG1 and JAG2 trafficking raise the possibility that
552 distinct assemblies of these ligands generate high, medium, and low Notch signaling
553 environments within the differentiating epithelium (Graphical Abstract). Further analysis of JAG
554 trafficking has the potential to identify treatments which could normalize goblet and ciliated cell
555 frequency in people who have chronic mucosecretory lung diseases and those whose ciliated
556 cell population is depleted by exposure to environmental agents.

557 **ACKNOWLEDGEMENTS**

558 This project was funded by a Research Grant from Cystic Fibrosis Foundation (REYNOL17XX0-
559 20XX0, SDR), the Nationwide Children's Hospital Cell Based Therapy Program (47306-0002-
560 1217, SDR), and a Nationwide Children's Hospital Technology Development Award
561 (Technology 2019-015, SDR). We acknowledge the Abigail Wexner Research Institute Center
562 for Genomics Research which conducted the RNA sequencing and analysis, and the C3 RDP
563 which provided human bronchial cells (MCCOY19R0). JAG1 and JAG2 neutralizing antibodies
564 were provided by Genentech, Inc. under a Materials Transfer Agreement.

565 **FIGURE LEGENDS**

566 *Graphical Abstract:* Different assemblies of JAG1 and JAG2 may determine Notch signal
567 strength and cell fate within the tracheobronchial epithelium. A cell which interacts with JAG1+
568 cells (blue squares) receives a low Notch signal (light yellow square). A cell which interacts with
569 a mixture of JAG1+ and JAG1+/JAG2+ cells (purple squares) receives a medium (med) Notch
570 signal (medium yellow square). A cell which interacts with JAG1+/JAG2+ cells receives a high
571 Notch signal (bright yellow square).

572 *Figure 1: Notch regulation of ciliated and goblet cell differentiation.* Human bronchial basal cells
573 were differentiated in air-liquid-interface cultures using H&H medium. Cells were treated with
574 vehicle (DMSO) or 25 μM DAPT as follows: treatment on differentiation days 0 and 2 and fix on
575 day 4, treatment on differentiation days 2 and 4 and fix on day 6, treatment on differentiation
576 days 4 and 6 and fix on day 8, or treatment on differentiation days 8 and 10 and fix on day 12.
577 Dual immunofluorescence was used to detect acetylated tubulin and MUC5B. Nuclei were
578 stained with DAPI. **A.** Frequency of cells with a primary cilium. **B.** Frequency of bristle cells. **C.**
579 Frequency of ciliated cells. **D.** Frequency of MUC5B-low cells. **E.** Frequency of MUC5B-medium
580 cells. **F.** Frequency of MUC5B-high cells. Mean ± SD, N=6.

581 *Figure 2: Impact of intermittent or continuous Notch inhibition of ciliated and goblet cell*
582 *differentiation.* **A-C***.* Human bronchial basal cells were differentiated in air-liquid-interface
583 cultures using H&H medium. Dual immunofluorescence was used to detect acetylated tubulin
584 and MUC5B. Nuclei were stained with DAPI. (**A)** Experimental design. Recovery study: Cells
585 were treated with 10 μM Ly on differentiation days 4 and 6 and with vehicle (DMSO) on
586 differentiation days 8 and 10. Cultures were fixed on day 12. Continuous study: Cells were
587 treated with 10 μM Ly on differentiation days 4, 6, 8, and 10. Cultures were fixed on day 12. (**B)**
588 Frequency of ciliated cell differentiation intermediates. P-cells with a primary cilium, B-bristle
589 cells, M-ciliated cells. (**C)** Frequency of goblet cell differentiation intermediates. L-MUC5B-low
590 cells, M-MUC5B-medium cells, H-MUC5B-high cells. Mean ± SD, N=3. **D-E**. Western blot
591 analysis of JAG1 (**D**) and JAG2 (**E**) abundance in cultures that were treated with DMSO, 10 μM
592 LY, or 25 μM DAPT on differentiation days 8 and 10 and harvested on differentiation day 12.
593 Mean ± SD, N=3.

594 *Figure 3: JAG1 subcellular location and length.* Human bronchial basal cells were differentiated
595 in air-liquid-interface cultures using H&H medium. **A-C.** Immunofluorescence was used to detect
596 JAG1 (red) on proliferation day 3 (**A**), differentiation day 2 (**B**), or differentiation day 4 (**C**).
597 Nuclei were detected with DAPI (blue). **D-E**. High magnification of the region indicated in panel

598 A. Arrows indicate JAG1 positive cells. **F-G.** Dual immunofluorescence analysis of JAG1 (green)
599 and β-catenin (β-Cat, red) on differentiation day 4. Nuclei were detected with DAPI (blue).
600 Three-color (**F**) and two color (**G**) images of the same region. **H.** Western blot analysis of JAG1
601 on differentiation days 4 and 8. The full-length band is labeled JAG1. Three samples per time
602 point. **I.** Cells were cultured to differentiation day 8, separated into cytoplasmic (C), nuclear (N),
603 insoluble (I) fractions, or were unfractionated (U), and proteins were analyzed by western blot.
604 Top panel: TOPOII, a nuclear protein; middle panel: alpha tubulin (αTUB), a cytoplasmic
605 protein; Bottom panel: JAG1. Two different samples were analyzed. **J.** Analysis of *Jag1* mRNA
606 abundance on differentiation days 2, 4, and 8. Mean ± SD (n=3). **K.** Western blot analysis of
607 JAG1 protein abundance. Mean ± SD (n=3).

608 *Figure 4: JAG2 subcellular location and length.* Human bronchial basal cells were differentiated
609 in air-liquid-interface cultures using H&H medium. **A-C.** Immunofluorescence was used to detect
610 JAG2 (red) and β-catenin (green) on proliferation day 5 (**A**), differentiation day 4 (**B**), or
611 differentiation day 8 (**C**). Nuclei were detected with DAPI (blue). Each panel presents single
612 color and merged images. Arrows: white, cortical JAG2; yellow, JAG2-high cells; blue, JAG2-
613 positive cells; pink, JAG2-negative cells. **D.** Immunofluorescence analysis of HES1 (red) and
614 RBPJK (red) on differentiation day 8. Nuclei were detected with DAPI (blue). **E.** Western blot
615 analysis of JAG2 on differentiation days 4 (lane 1) and 8 (lane 2). The full-length band is labeled
616 JAG2. **F**. Co-immunoprecipitation analysis of JAG2 and β-catenin on differentiation day 8.
617 Proteins were immunoprecipitated with an N-terminus (N-term) specific β-catenin antibody.
618 Precipitates were analyzed for β-catenin using a C-terminus (C-term) specific β-catenin
619 antibody, N-term specific β-catenin antibody, or a JAG2 N-term specific antibody. Three
620 samples were analyzed. **G.** Analysis of *Jag2* mRNA abundance on differentiation days 2, 4, and
621 8. Mean ± SD (n=3). **H.** Western blot analysis of JAG2 protein abundance. Mean ± SD, N=3. **G.**

622 *Figure 5: Regulation of JAG1 and JAG2 abundance.* Human bronchial basal cells were
623 differentiated in air-liquid-interface cultures using H&H medium. **A-B.** On differentiation days 4
624 and 6, the cultures were treated with vehicle, (Veh, DMSO), CHIR99021 (CHIR), XAV939
625 (XAV), or LGK974 (LGK) and protein lysates were collected on day 8. Drug concentrations are
626 in μM. Western blots were used to quantify JAG1 (**A**) and JAG2 (**B**) abundance. Mean ± SD,
627 N=3. **C-D.** Cultures were treated with Veh or DKK1 on differentiation days 0 and 2 and lysed on
628 day 4 or treated on differentiation days 4 and 6 and lysed on day 8. Drug concentrations are in
629 ng/ml. Western blots were used to quantify JAG1 (**C**) and JAG2 (**D**) abundance. Mean ± SD,
630 N=3. **E-F**. Uniform manifold approximation and projection (UMAP) analysis of cells that were

631 treated with vehicle (**E**) or CHIR (**F**) on days 4 and 6 and harvested for scRNAseq analysis on
632 day 8. **G.** Number of normalized cells per Surat Cluster.

633 *Figure 6: JAG1 and JAG2 trafficking to the cell surface.* Human bronchial basal cells were
634 differentiated in air-liquid-interface cultures using H&H medium. **A-B**. On differentiation day 8,
635 cultures were fixed under non-permeabilization conditions and JAG1 (green) and JAG2 (red)
636 were detected by dual immunofluorescence staining. Nuclei were stained with DAPI (blue).
637 Panel B is a higher magnification of the region indicated in panel A. **C-F.** After imaging, the
638 cultures were permeabilized and re-stained for JAG1 (green), JAG2 (red), and DAPI (blue).
639 Arrows: antigen-positive cells. **G.** On differentiation day 8, cell surface proteins were labeled
640 with biotin, biotinylated proteins were recovered, and the bound (BIO) and unbound (UnB)
641 fractions were evaluated by western blot. Two samples were evaluated. **H.** On differentiation
642 day 8, cell lysates were reacted with TUBE beads which bind to proteins decorated with 4 or
643 more ubiquitin moieties. The bound fraction was treated with vehicle (-DUB) or a broad
644 spectrum debubiquitinase (+DUB). Western blots were generated from the unfractionated (In),
645 unbound (Un), -DUB, and +DUB samples and were evaluated for JAG1 and JAG2.
646 *Ubiquitinated JAG2, **deubiquitinated JAG2. Immunofluorescence was used to detect JAG2 in
647 Veh (**I**) and CHIR (5 μM, **J**) treated cultures on differentiation day 8. Arrows: red, JAG2-high cell;
648 white, JAG2-negative cell; yellow, redistributed JAG2. Asterisks: JAG2-low cells. **K.** Cells were
649 cultured to differentiation day 8, lysed, and immunoprecipitated with a phospho-serine/phospho-
650 threonine (pSer/pThr) antibody. Precipitates were analyzed for JAG2 using the C-terminus
651 specific antibody, KRT5 antibody, or a pan-YWHA antibody. Two samples were analyzed.

652 *Figure 7: Roles for JAG1 and JAG2 in ciliated and goblet cell differentiation.* Human bronchial
653 basal cells were differentiated in air-liquid-interface cultures using H&H medium. Treatments
654 were on differentiation days 8 and 10 and cultures were fixed on day 12. Differentiation was
655 quantified by immunofluorescence analysis of acetylated tubulin, MUC5B, and DAPI. **A-B.** Cells
656 were treated with vehicle (DMSO) or 40 μM JAG1 peptide. Frequency of ciliated cell
657 differentiation intermediates. P-cells with a primary cilium, B-bristle cells, M-ciliated cells (**A**).
658 Frequency of goblet cell differentiation intermediates (**B**). L-MUC5B-low cells, M-MUC5B-
659 medium cells, H-MUC5B-high cells. **C-F.** Cells were treated with vehicle (PBS) or 25 μg/ml
660 neutralizing antibody to JAG1 (αJ1) or JAG2 (αJ2). Frequency of bristle cells (**C**). Frequency of
661 ciliated cells (**D**). Frequency of MUC5B-medium cells (**E**). Frequency of MUC5B-high cells (**F**).
662 **G-J.** Cells were treated with PBS or 25 μg/ml αJ1 and 25 μg/ml αJ2. Frequency of bristle cells

663 (**G**). Frequency of ciliated cells (**H**). Frequency of MUC5B-medium cells (**I**). Frequency of
664 MUC5B-high cells (**J**). Mean ± SD, N=6.

665 *Supplemental Figure 1: Ciliated and goblet cell differentiation as a function of medium type.*
666 Human bronchial basal cells were differentiated in air-liquid-interface cultures using three
667 media: Wu, H&H (H&H), and complete Pneumacult (cPC). Cultures were fixed on days 7 and
668 14. **A.** Cell density was determined by quantifying the number of DAPI-stained nuclei per unit
669 area. **B.** Ciliated cells were identified by acetylated tubulin (ACT) staining and their frequency
670 was reported as the number ACT+ cells/number nuclei. **C.** Goblet cells were identified by
671 MUC5B staining and their frequency was reported as the number MUC5B+ cells/number nuclei.
672 Mean ± SD, N=6.

673 *Supplemental Figure 2: Intermediate ciliated and goblet cell phenotypes.* Human bronchial basal
674 cells were differentiated in air-liquid-interface cultures using H&H medium. **A-B.** Cells defined by
675 a primary cilium were identified by ACT staining on differentiation day 4. Panel B is a high
676 magnification image of the region identified in panel A. Arrows: white, primary cilium; yellow,
677 mitotic figure. **C-D.** Cells with bristle morphology were identified by ACT staining on
678 differentiation day 8. Panel D is a high magnification image of the region identified in panel C.
679 Arrows: bristle cells. **E-F.** Ciliated cells defined were identified by ACT staining on differentiation
680 day 12. Panel F is a high magnification image of the region identified in panel E. Arrows:
681 Ciliated cells. G-H. Goblet cells were identified by MUC5B staining on differentiation day 8.
682 Panel H is a high magnification image of the region identified in panel G. Arrows identify
683 MUC5B-low, -medium, and -high goblet cell intermediates.

684 *Supplemental Figure 3: Cell density in vehicle and DAPT treated cultures.* Human bronchial
685 basal cells were differentiated in air-liquid-interface cultures using H&H medium. Cells were
686 treated with vehicle (DMSO) or 25 μM DAPT as follows: treatment on differentiation days 0 and
687 2 and fix on day 4, treatment on differentiation days 2 and 4 and fix on day 6, treatment on
688 differentiation days 4 and 6 and fix on day 8, or treatment on differentiation days 8 and 10 and
689 fix on day 12. Nuclei were stained with DAPI and quantified. Mean ± SD, N=6.

690 *Supplemental Figure 4: JAG1 and JAG2 localization as a function of medium type.* Human
691 bronchial basal cells were differentiated in air-liquid-interface cultures using three media: Wu (**A,**
692 **D, G, J**), H&H (H&H, **B, E, H, K**), and complete Pneumacult (cPC, **C, F, I, L**). Cultures were
693 fixed on day 7. JAG1 (green, **A-C**) and JAG2 (red, **D-F**) were detected by dual
694 immunofluorescence. Nuclei were detected with DAPI (blue, **G-I**). Merged images (**J-L**). Arrows:
695 yellow, JAG2 expression; white, low JAG2 expression. Scale bar in panel A, 100 μm.

696 *Supplemental Figure 5: Gene expression and gene set enrichment analysis.* ALI cultures were
697 treated with vehicle, 10 μM CHIR or 10 μM XAV on differentiation days 4 and 6 and RNA was
698 purified on day 8. Transcriptional changes were interrogated by RNA-sequencing and Gene Set
699 Expression Analysis (GSEA). **A.** GSEA for WNT/β-catenin genes in vehicle and CHIR treated
700 cultures. **B.** Heat map representation of WNT/β-catenin genes in vehicle and CHIR treated
701 cultures. Each column is a sample: samples 1-3 vehicle treated (VEH), samples 4-6 CHIR
702 treated. Each row is a gene. Red indicates upregulation. Blue indicates downregulation.
703 Leading-edge genes are indicated by the green line. Jag1 and Jag2 are indicated by the
704 asterisks. **C.** GSEA for WNT/β-catenin genes in vehicle and XAV treated cultures. **D.** Heat map
705 representation of WNT/β-catenin genes in vehicle and XAV treated cultures. Each column is a
706 sample: samples 1-3 vehicle (VEH treated), samples 7-9 XAV treated. Each row is a gene. Red
707 indicates upregulation. Blue indicates downregulation. Leading-edge genes are indicated by the
708 green line. Jag1 and Jag2 are indicated by the asterisks. **E.** GSEA for Notch genes in vehicle
709 and CHIR treated cultures. **F.** Heat map representation of Notch genes in vehicle and CHIR
710 treated cultures. Each column is a sample: samples 1-3 vehicle (VEH treated), samples 4-6
711 CHIR treated. Each row is a gene. Red indicates upregulation. Blue indicates downregulation.
712 Leading-edge genes are indicated by the green line. Jag1 and Jag2 are indicated by the
713 asterisks. **G.** GSEA for Notch genes in vehicle and XAV treated cultures. **H.** Heat map
714 representation of Notch genes in vehicle and XAV treated cultures. Each column is a sample:
715 samples 1-3 vehicle (VEH treated), samples 7-9 XAV treated. Each row is a gene. Red
716 indicates upregulation. Blue indicates downregulation. Leading-edge genes are indicated by the
717 green line. Jag1 and Jag2 are indicated by the asterisks. **I.** Analysis of *Jag1* gene expression in
718 vehicle, CHIR, and XAV treated cultures. Data are presented as the Log2(fold change). Mean ±
719 SD (n=3). No significant differences were detected. **J.** Analysis of *Jag2* gene expression in
720 vehicle, CHIR, and XAV treated cultures. Data are presented as the Log2(fold change). Mean ±
721 SD (n=3). No significant differences were detected.

722 *Supplemental Figure 6: Analysis of leading-edge genes.* ALI cultures were treated with vehicle,
723 10 μM CHIR or 10 μM XAV on differentiation days 4 and 6 and RNA was purified on day 8.
724 Transcriptional changes were interrogated by RNA-sequencing and Gene Set Expression
725 Analysis (GSEA). Leading-edge genes, which determine the gene set Enrichment Score, were
726 extracted and organized to indicate similarities/differences across the treatments and gene sets.
727 Red indicates downregulation. Blue indicates upregulation. Transc: Transcriptional targets of
728 WNT/β-catenin were based on literature reports. (transc): WNT/β-catenin targets identified by

729 similarity. Protein: Targets of glycogen synthase kinase (GSK3) and tankyrase (TNKS) were
730 based on literature reports. (protein): GSK3 and TNKS targets identified by similarity.

731 *Supplemental Figure 7:* Roles for JAG1 and JAG2 in tracheobronchial cell fate decisions. **A**.
732 JAG1 or JAG2 permit Basal Progenitor Cell (BPC) differentiation to a Secretory Progenitor Cell
733 (SPC) and SPC differentiation to a bristle cell (green light). Both JAG1 and JAG2 are required
734 for SPC differentiation to a goblet cell (green light). **B**. JAG2 inhibits the Squamous Cell fate
735 (red light). **C.** JAG2 pauses progression from one ciliated cell differentiation intermediate to the
736 next (yellow light).

737 **REFERENCES**


738 1. Hong KU, Reynolds SD, Watkins S, Fuchs E, Stripp BR. Basal cells are a multipotent
739 progenitor capable of renewing the bronchial epithelium. The American journal of pathology.
740 2004;164(2):577-88.

741 2. Hong KU, Reynolds SD, Watkins S, Fuchs E, Stripp BR. In vivo differentiation potential
742 of tracheal basal cells: Evidence for multipotent and unipotent subpopulations. American journal
743 of physiology Lung cellular and molecular physiology. 2003.

744 3. Ghosh M, Brechbuhl HM, Smith RW, Li B, Hicks DA, Titchner T, et al. Context-
745 dependent differentiation of multipotential keratin 14-expressing tracheal basal cells. American
746 journal of respiratory cell and molecular biology. 2011;45(2):403-10.

747 4. Rock JR, Onaitis MW, Rawlins EL, Lu Y, Clark CP, Xue Y, et al. Basal cells as stem
748 cells of the mouse trachea and human airway epithelium. Proceedings of the National Academy
749 of Sciences of the United States of America. 2009;106(31):12771-5.

750 5. Engelhardt JF, Schlossberg H, Yankaskas JR, Dudus L. Progenitor cells of the adult
751 human airway involved in submucosal gland development. Development. 1995;121(7):2031-46.

752 6. Carraro G, Stripp BR. A new notch for lung stem cells. Cell stem cell. 2015;16(2):107-9.

753 7. Kiyokawa H, Morimoto M. Notch signaling in the mammalian respiratory system,
754 specifically the trachea and lungs, in development, homeostasis, regeneration, and disease.
755 Dev Growth Differ. 2020;62(1):67-79.

756 8. Radtke F, Raj K. The role of Notch in tumorigenesis: oncogene or tumour suppressor?
757 Nature reviews Cancer. 2003;3(10):756-67.
758 9. Kopan R, Ilagan MX. The canonical Notch signaling pathway: unfolding the activation
759 mechanism. Cell. 2009;137(2):216-33.
760 10. Ilagan MX, Kopan R. SnapShot: notch signaling pathway. Cell. 2007;128(6):1246.
761 11. Castel D, Mourikis P, Bartels SJ, Brinkman AB, Tajbakhsh S, Stunnenberg HG. Dynamic
762 binding of RBPJ is determined by Notch signaling status. Genes & development.
763 2013;27(9):1059-71.
764 12. Vieira Braga FA, Kar G, Berg M, Carpaij OA, Polanski K, Simon LM, et al. A cellular
765 census of human lungs identifies novel cell states in health and in asthma. Nature medicine.
766 2019;25(7):1153-63.
767 13. Carraro G, Mulay A, Yao C, Mizuno T, Konda B, Petrov M, et al. Single Cell
768 Reconstruction of Human Basal Cell Diversity in Normal and IPF Lung. American journal of
769 respiratory and critical care medicine. 2020.
770 14. Goldfarbmuren KC, Jackson ND, Sajuthi SP, Dyjack N, Li KS, Rios CL, et al. Dissecting
771 the cellular specificity of smoking effects and reconstructing lineages in the human airway
772 epithelium. Nature communications. 2020;11(1):2485.
773 15. Bodas M, Moore AR, Subramaniyan B, Georgescu C, Wren JD, Freeman WM, et al.
774 Cigarette Smoke Activates NOTCH3 to Promote Goblet Cell Differentiation in Human Airway
775 Epithelial Cells. American journal of respiratory cell and molecular biology. 2021;64(4):426-40.
776 16. Verhein KC, McCaw Z, Gladwell W, Trivedi S, Bushel PR, Kleeberger SR. Novel Roles
777 for Notch3 and Notch4 Receptors in Gene Expression and Susceptibility to Ozone-Induced
778 Lung Inflammation in Mice. Environmental health perspectives. 2015;123(8):799-805.
779 17. Xu F, Gao J, Bergmann S, Sims AC, Ashbrook DG, Baric RS, et al. Genetic Dissection
780 of the Regulatory Mechanisms of Ace2 in the Infected Mouse Lung. Front Immunol.
781 2020;11:607314.

782 18. Qin L, Qiu KZ, Hu CP, Wu GJ, Wang LL, Tan YR. Bronchial Epithelial Cells Promote the
783 Differentiation of Th2 Lymphocytes in Airway Microenvironment through Jagged/Notch-1
784 Signaling after RSV Infection. Int Arch Allergy Immunol. 2019;179(1):43-52.
785 19. Tsao PN, Wei SC, Wu MF, Huang MT, Lin HY, Lee MC, et al. Notch signaling prevents
786 mucous metaplasia in mouse conducting airways during postnatal development. Development.
787 2011;138(16):3533-43.
788 20. Morimoto M, Nishinakamura R, Saga Y, Kopan R. Different assemblies of Notch
789 receptors coordinate the distribution of the major bronchial Clara, ciliated and neuroendocrine
790 cells. Development. 2012;139(23):4365-73.
791 21. Rock JR, Gao X, Xue Y, Randell SH, Kong YY, Hogan BL. Notch-dependent
792 differentiation of adult airway basal stem cells. Cell stem cell. 2011;8(6):639-48.
793 22. Gomi K, Arbelaez V, Crystal RG, Walters MS. Activation of NOTCH1 or NOTCH3
794 signaling skews human airway basal cell differentiation toward a secretory pathway. PloS one.
795 2015;10(2):e0116507.
796 23. Reid AT, Nichol KS, Chander Veerati P, Moheimani F, Kicic A, Stick SM, et al. Blocking
797 Notch3 Signaling Abolishes MUC5AC Production in Airway Epithelial Cells from Individuals with
798 Asthma. American journal of respiratory cell and molecular biology. 2020;62(4):513-23.
799 24. Stupnikov MR, Yang Y, Mori M, Lu J, Cardoso WV. Jagged and Delta-like ligands
800 control distinct events during airway progenitor cell differentiation. eLife. 2019;8.
801 25. Paul MK, Bisht B, Darmawan DO, Chiou R, Ha VL, Wallace WD, et al. Dynamic changes
802 in intracellular ROS levels regulate airway basal stem cell homeostasis through Nrf2-dependent
803 Notch signaling. Cell stem cell. 2014;15(2):199-214.
804 26. Mori M, Mahoney JE, Stupnikov MR, Paez-Cortez JR, Szymaniak AD, Varelas X, et al.
805 Notch3-Jagged signaling controls the pool of undifferentiated airway progenitors. Development.
806 2015;142(2):258-67.

807 27. Gomi K, Staudt MR, Salit J, Kaner RJ, Heldrich J, Rogalski AM, et al. JAG1-Mediated
808 Notch Signaling Regulates Secretory Cell Differentiation of the Human Airway Epithelium. Stem
809 Cell Rev Rep. 2016;12(4):454-63.
810 28. Zhang S, Loch AJ, Radtke F, Egan SE, Xu K. Jagged1 is the major regulator of Notch-
811 dependent cell fate in proximal airways. Developmental dynamics : an official publication of the
812 American Association of Anatomists. 2013;242(6):678-86.
813 29. Lafkas D, Shelton A, Chiu C, de Leon Boenig G, Chen Y, Stawicki SS, et al. Therapeutic
814 antibodies reveal Notch control of transdifferentiation in the adult lung. Nature.
815 2015;528(7580):127-31.
816 30. Carrer M, Crosby JR, Sun G, Zhao C, Damle SS, Kuntz SG, et al. Antisense
817 Oligonucleotides Targeting Jagged 1 Reduce House Dust Mite-induced Goblet Cell Metaplasia
818 in the Adult Murine Lung. American journal of respiratory cell and molecular biology.
819 2020;63(1):46-56.
820 31. Plasschaert LW, Zilionis R, Choo-Wing R, Savova V, Knehr J, Roma G, et al. A single-
821 cell atlas of the airway epithelium reveals the CFTR-rich pulmonary ionocyte. Nature.
822 2018;560(7718):377-81.
823 32. Montoro DT, Haber AL, Biton M, Vinarsky V, Lin B, Birket SE, et al. A revised airway
824 epithelial hierarchy includes CFTR-expressing ionocytes. Nature. 2018;560(7718):319-24.
825 33. Jain R, Pan J, Driscoll JA, Wisner JW, Huang T, Gunsten SP, et al. Temporal
826 relationship between primary and motile ciliogenesis in airway epithelial cells. American journal
827 of respiratory cell and molecular biology. 2010;43(6):731-9.
828 34. Boutin C, Kodjabachian L. Biology of multiciliated cells. Current opinion in genetics &
829 development. 2019;56:1-7.
830 35. Malleske DT, Hayes D, Jr., Lallier SW, Hill CL, Reynolds SD. Regulation of human
831 airway epithelial tissue stem cell differentiation by beta-catenin, P300, and CBP. Stem Cells.
832 2018.

833 36. Seibold MA, Smith RW, Urbanek C, Groshong SD, Cosgrove GP, Brown KK, et al. The
834 idiopathic pulmonary fibrosis honeycomb cyst contains a mucocilary pseudostratified epithelium.
835 PloS one. 2013;8(3):e58658.
836 37. Fulcher ML, Randell SH. Human nasal and tracheo-bronchial respiratory epithelial cell
837 culture. Methods Mol Biol. 2013;945:109-21.
838 38. Hayes D, Jr., Kopp BT, Hill CL, Lallier SW, Schwartz CM, Tadesse M, et al. Cell Therapy
839 for Cystic Fibrosis Lung Disease: Regenerative Basal Cell Amplification. Stem Cells Transl Med.
840 2018.
841 39. Reynolds SD, Rios C, Wesolowska-Andersen A, Zhuang Y, Pinter M, Happoldt C, et al.
842 Airway Progenitor Clone Formation is Enhanced by Y-27632-dependent Changes in the
843 Transcriptome. American journal of respiratory cell and molecular biology. 2016.
844 40. Suprynowicz FA, Upadhyay G, Krawczyk E, Kramer SC, Hebert JD, Liu X, et al.
845 Conditionally reprogrammed cells represent a stem-like state of adult epithelial cells.
846 Proceedings of the National Academy of Sciences of the United States of America.
847 2012;109(49):20035-40.
848 41. Wu R. Culture of normal human airway epithelial cells and measurement of mucin
849 synthesis and secretion. Methods in molecular medicine. 2000;44:31-9.
850 42. Lallier SW, Hill CL, Nichols DP, Reynolds SD. Protein Abundance Determination: An
851 Optimized Western Blot Workflow. Ann Clin Lab Sci. 2019;49(4):507-12.
852 43. Carraro G, Langerman J, Sabri S, Lorenzana Z, Purkayastha A, Zhang G, et al.
853 Transcriptional analysis of cystic fibrosis airways at single-cell resolution reveals altered
854 epithelial cell states and composition. Nature medicine. 2021;27(5):806-14.
855 44. Young MD, Behjati S. SoupX removes ambient RNA contamination from droplet-based
856 single-cell RNA sequencing data. Gigascience. 2020;9(12).
857 45. Wolock SL, Lopez R, Klein AM. Scrublet: Computational Identification of Cell Doublets in
858 Single-Cell Transcriptomic Data. Cell Syst. 2019;8(4):281-91 e9.

859 46. Lun AT, McCarthy DJ, Marioni JC. A step-by-step workflow for low-level analysis of
860 single-cell RNA-seq data with Bioconductor. F1000Res. 2016;5:2122.
861 47. Wolf FA, Hamey FK, Plass M, Solana J, Dahlin JS, Gottgens B, et al. PAGA: graph
862 abstraction reconciles clustering with trajectory inference through a topology preserving map of
863 single cells. Genome biology. 2019;20(1):59.
864 48. Becht E, McInnes L, Healy J, Dutertre CA, Kwok IWH, Ng LG, et al. Dimensionality
865 reduction for visualizing single-cell data using UMAP. Nature biotechnology. 2018.
866 49. Finak G, McDavid A, Yajima M, Deng J, Gersuk V, Shalek AK, et al. MAST: a flexible
867 statistical framework for assessing transcriptional changes and characterizing heterogeneity in
868 single-cell RNA sequencing data. Genome biology. 2015;16:278.
869 50. Tirosh I, Izar B, Prakadan SM, Wadsworth MH, 2nd, Treacy D, Trombetta JJ, et al.
870 Dissecting the multicellular ecosystem of metastatic melanoma by single-cell RNA-seq.
871 Science. 2016;352(6282):189-96.
872 51. LaVoie MJ, Selkoe DJ. The Notch ligands, Jagged and Delta, are sequentially
873 processed by alpha-secretase and presenilin/gamma-secretase and release signaling
874 fragments. The Journal of biological chemistry. 2003;278(36):34427-37.
875 52. Ikeuchi T, Sisodia SS. The Notch ligands, Delta1 and Jagged2, are substrates for
876 presenilin-dependent "gamma-secretase" cleavage. The Journal of biological chemistry.
877 2003;278(10):7751-4.
878 53. Metrich M, Bezdek Pomey A, Berthonneche C, Sarre A, Nemir M, Pedrazzini T. Jagged1
879 intracellular domain-mediated inhibition of Notch1 signalling regulates cardiac homeostasis in
880 the postnatal heart. Cardiovasc Res. 2015;108(1):74-86.
881 54. An WF, Germain AR, Bishop JA, Nag PP, Metkar S, Ketterman J, et al. Discovery of
882 Potent and Highly Selective Inhibitors of GSK3b. Probe Reports from the NIH Molecular
883 Libraries Program. Bethesda (MD)2010.

884 55. Huang SM, Mishina YM, Liu S, Cheung A, Stegmeier F, Michaud GA, et al. Tankyrase
885 inhibition stabilizes axin and antagonizes Wnt signalling. Nature. 2009;461(7264):614-20.
886 56. Araya J, Cambier S, Markovics JA, Wolters P, Jablons D, Hill A, et al. Squamous
887 metaplasia amplifies pathologic epithelial-mesenchymal interactions in COPD patients. The
888 Journal of clinical investigation. 2007;117(11):3551-62.
889 57. Sun J, Luo Z, Wang G, Wang Y, Wang Y, Olmedo M, et al. Notch ligand Jagged1
890 promotes mesenchymal stromal cell-based cartilage repair. Exp Mol Med. 2018;50(9):1-10.
891 58. Dontu G, Jackson KW, McNicholas E, Kawamura MJ, Abdallah WM, Wicha MS. Role of
892 Notch signaling in cell-fate determination of human mammary stem/progenitor cells. Breast
893 Cancer Res. 2004;6(6):R605-15.
894 59. Hellstrom M, Phng LK, Hofmann JJ, Wallgard E, Coultas L, Lindblom P, et al. Dll4
895 signalling through Notch1 regulates formation of tip cells during angiogenesis. Nature.
896 2007;445(7129):776-80.
897 60. Ezratty EJ, Pasolli HA, Fuchs E. A Presenilin-2-ARF4 trafficking axis modulates Notch
898 signaling during epidermal differentiation. The Journal of cell biology. 2016;214(1):89-101.
899 61. Tan FE, Vladar EK, Ma L, Fuentealba LC, Hoh R, Espinoza FH, et al. Myb promotes
900 centriole amplification and later steps of the multiciliogenesis program. Development.
901 2013;140(20):4277-86.
902 62. El-Osta MA, Idkowiak-Baldys J, Hannun YA. Delayed phosphorylation of classical
903 protein kinase C (PKC) substrates requires PKC internalization and formation of the pericentrion
904 in a phospholipase D (PLD)-dependent manner. The Journal of biological chemistry.
905 2011;286(22):19340-53.
906 63. Fortini ME, Bilder D. Endocytic regulation of Notch signaling. Current opinion in genetics
907 & development. 2009;19(4):323-8.

908 64. Taelman VF, Dobrowolski R, Plouhinec JL, Fuentealba LC, Vorwald PP, Gumper I, et al.
909 Wnt signaling requires sequestration of glycogen synthase kinase 3 inside multivesicular
910 endosomes. Cell. 2010;143(7):1136-48.
911 65. Vinyoles M, Del Valle-Perez B, Curto J, Vinas-Castells R, Alba-Castellon L, Garcia de
912 Herreros A, et al. Multivesicular GSK3 sequestration upon Wnt signaling is controlled by p120-
913 catenin/cadherin interaction with LRP5/6. Molecular cell. 2014;53(3):444-57.
914 66. Zheng L, Conner SD. Glycogen synthase kinase 3beta inhibition enhances Notch1
915 recycling. Molecular biology of the cell. 2018;29(4):389-95.
916 67. de Carvalho A, Strikoudis A, Liu HY, Chen YW, Dantas TJ, Vallee RB, et al. Glycogen
917 synthase kinase 3 induces multilineage maturation of human pluripotent stem cell-derived lung
918 progenitors in 3D culture. Development. 2019;146(2).
919

Graphical Abstract

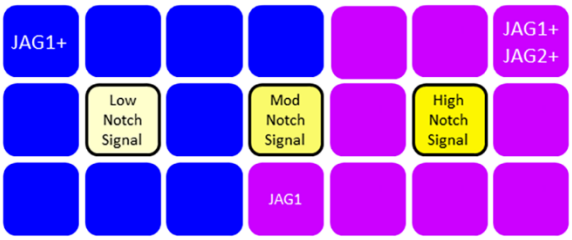

Figure 1

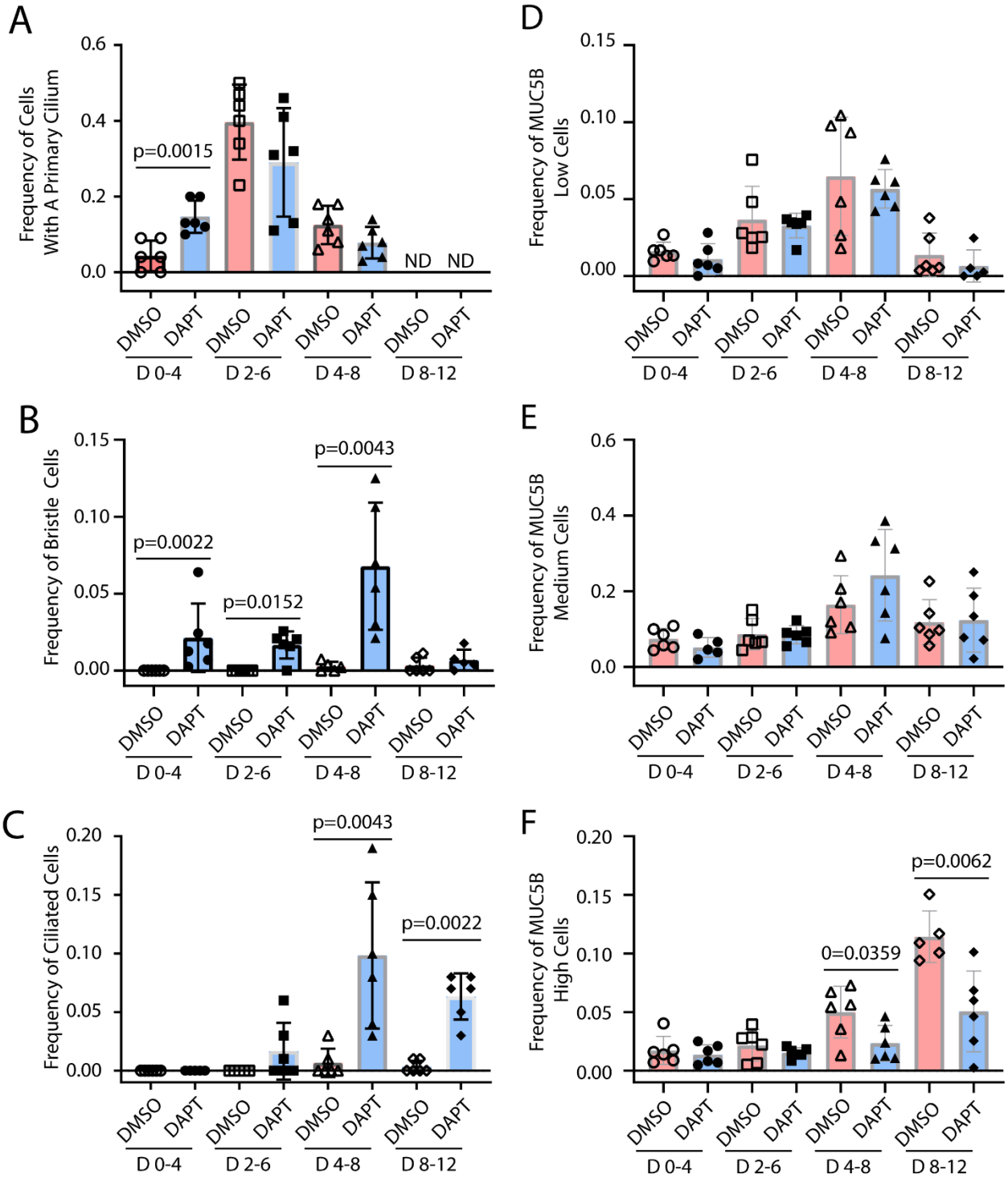
A
Frequency of Cells With A Primary Cilium
0.6
0.4
0.2
0.0
p=0.0015
ND
ND
DMSO
DAPT
D 0-4
D 2-6
D 4-8
D 8-12
B
Frequency of Bristle Cells
0.15
0.10
0.05
0.00
p=0.0022
p=0.0152
p=0.0043
C
Frequency of Ciliated Cells
0.20
0.15
0.10
0.05
0.00
p=0.0043
p=0.0022
D
Frequency of MUC5B Low Cells
E
Frequency of MUC5B Medium Cells
F
Frequency of MUC5B High Cells
0=0.0359
p=0.0062

Figure 2

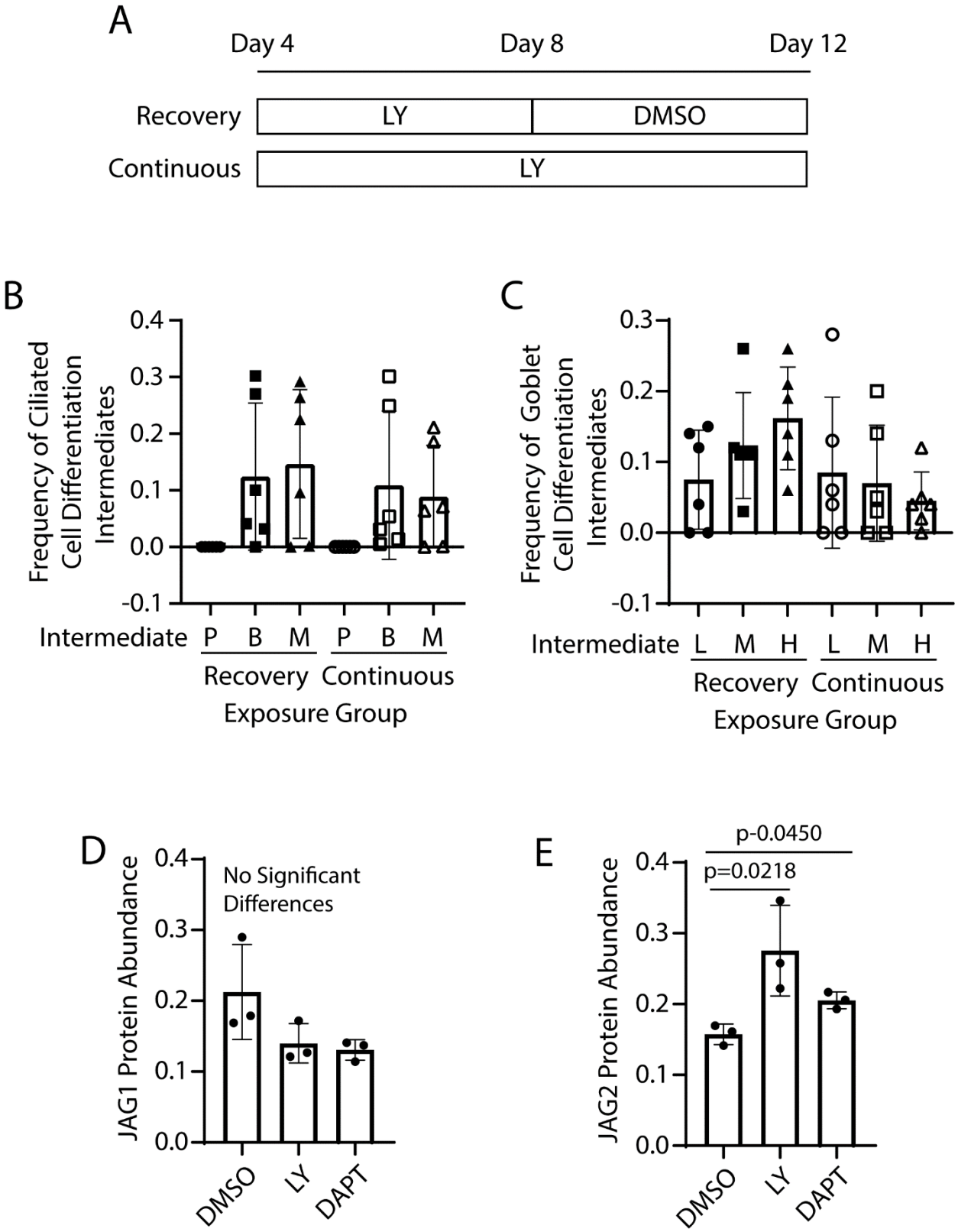
A
Day 4
Day 8
Day 12
Recovery
LY
DMSO
Continuous
LY
B
Frequency of Ciliated Cell Differentiation Intermediates
0.4
0.3
0.2
0.1
0.0
-0.1
Intermediate
P
B
M
P
B
M
Recovery
Continuous
Exposure Group
C
Frequency of Goblet Cell Differentiation Intermediates
0.3
0.2
0.1
0.0
-0.1
Intermediate
L
M
H
L
M
H
Recovery
Continuous
Exposure Group
D
JAG1 Protein Abundance
0.4
0.3
0.2
0.1
0.0
No Significant Differences
DMSO
LY
DAPT
E
JAG2 Protein Abundance
p-0.0450
p=0.0218
0.4
0.3
0.2
0.1
0.0
DMSO
LY
DAPT

Figure 3

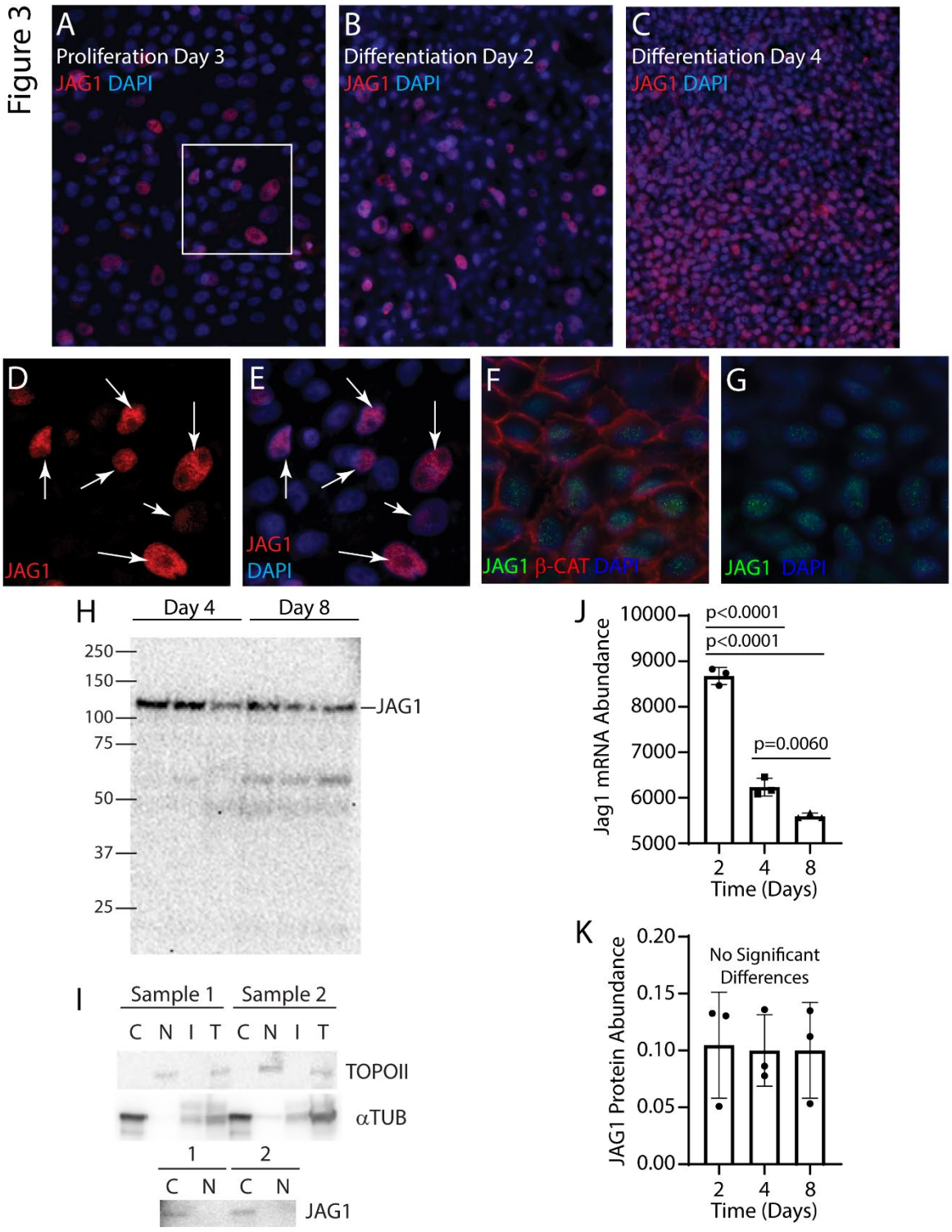
A
Proliferation Day 3
JAG1 DAPI
B
Differentiation Day 2
JAG1 DAPI
C
Differentiation Day 4
JAG1 DAPI
D
JAG1
E
JAG1
DAPI
F
JAG1 β-CAT DAPI
G
JAG1 DAPI
H
Day 4
Day 8
250
150
100
75
50
37
25
JAG1
I
Sample 1
Sample 2
C N I T C N I T
TOPOII
αTUB
1
2
C N C N
JAG1
J
Jag1 mRNA Abundance
10000
9000
8000
7000
6000
5000
p<0.0001
p<0.0001
p=0.0060
2 4 8
Time (Days)
K
JAG1 Protein Abundance
0.20
0.15
0.10
0.05
0.00
No Significant Differences
2 4 8
Time (Days)

Figure 4

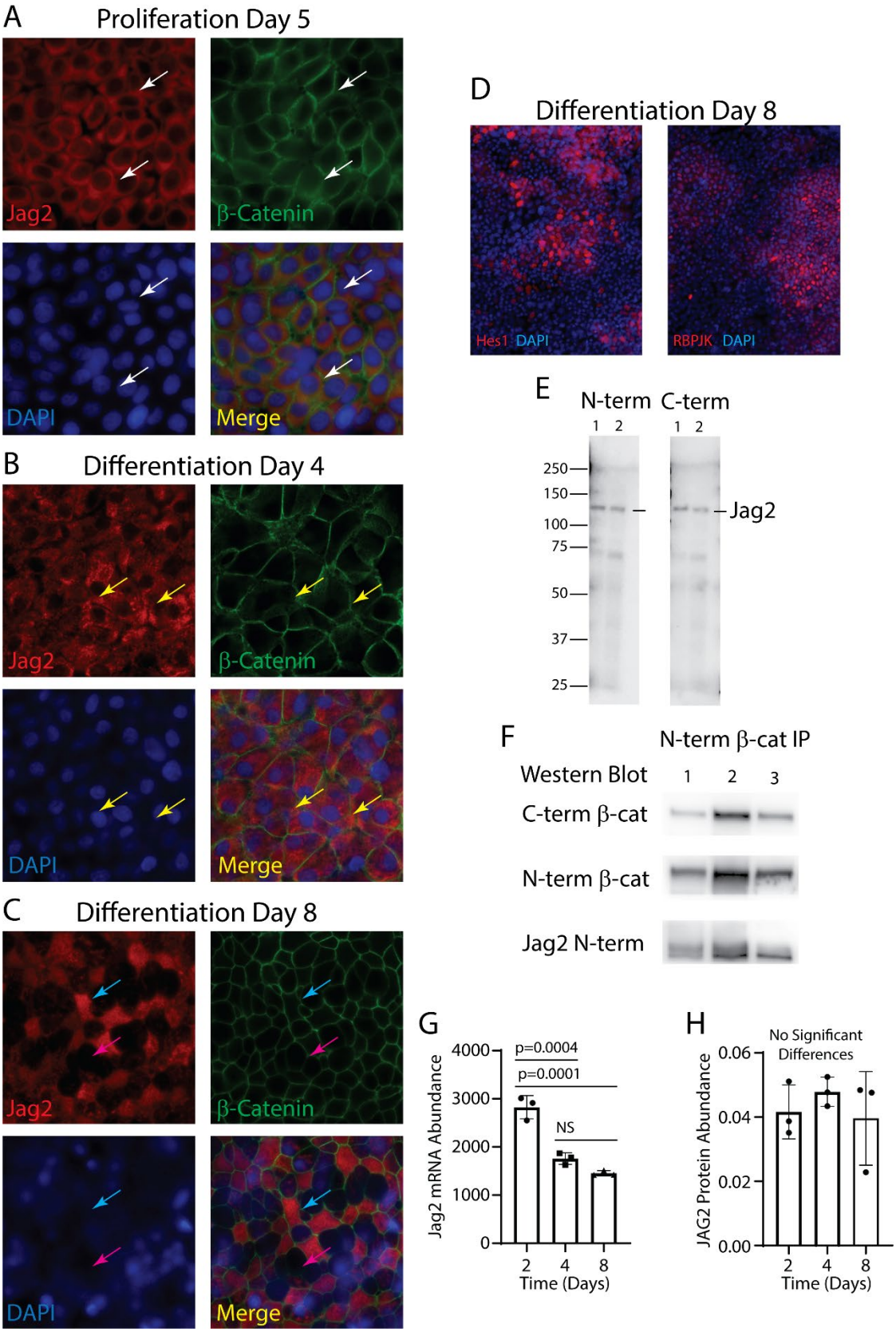
A
Proliferation Day 5
Jag2
β-Catenin
DAPI
Merge
B
Differentiation Day 4
Jag2
β-Catenin
DAPI
Merge
C
Differentiation Day 8
Jag2
β-Catenin
DAPI
Merge
D
Differentiation Day 8
Hes1 DAPI
RBPJK DAPI
E
N-term C-term
1 2 1 2
250
150
100
75
50
37
25
Jag2
F
N-term β-cat IP
Western Blot
1 2 3
C-term β-cat
N-term β-cat
Jag2 N-term
G
Jag2 mRNA Abundance
4000
3000
2000
1000
0
p=0.0004
p=0.0001
NS
2 4 8
Time (Days)
H
No Significant Differences
JAG2 Protein Abundance
0.06
0.04
0.02
0.00
2 4 8
Time (Days)

Figure 5

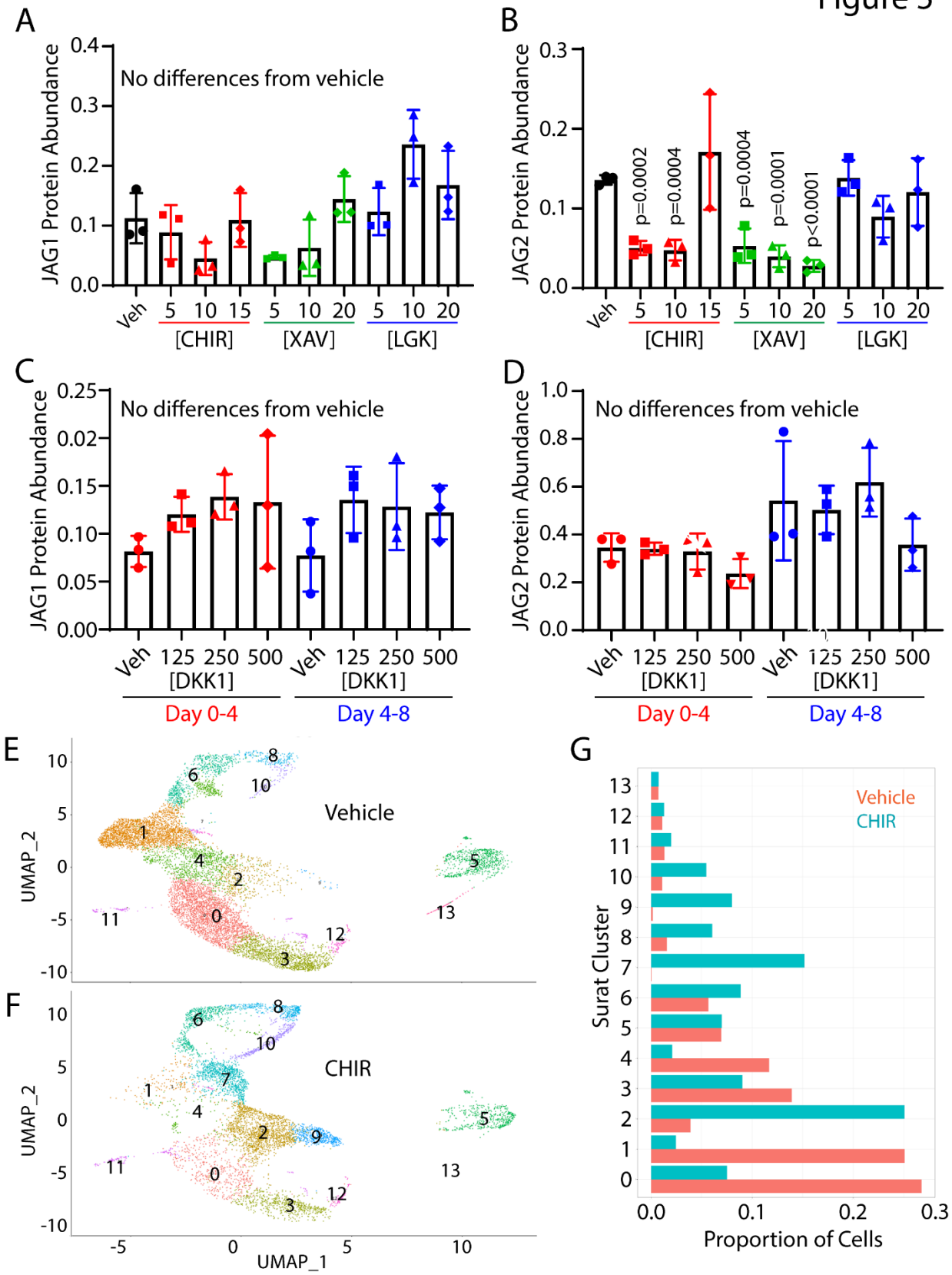
A
JAG1 Protein Abundance
No differences from vehicle
Veh
5 10 15
[CHIR]
5 10 20
[XAV]
5 10 20
[LGK]
B
JAG2 Protein Abundance
p=0.0002
p=0.0004
p=0.0004
p=0.0001
p<0.0001
C
JAG1 Protein Abundance
No differences from vehicle
Veh 125 250 500
[DKK1]
Day 0-4
Day 4-8
D
JAG2 Protein Abundance
No differences from vehicle
E
Vehicle
UMAP_2
F
CHIR
UMAP_1
G
Vehicle
CHIR
Surat Cluster
Proportion of Cells

Figure 6

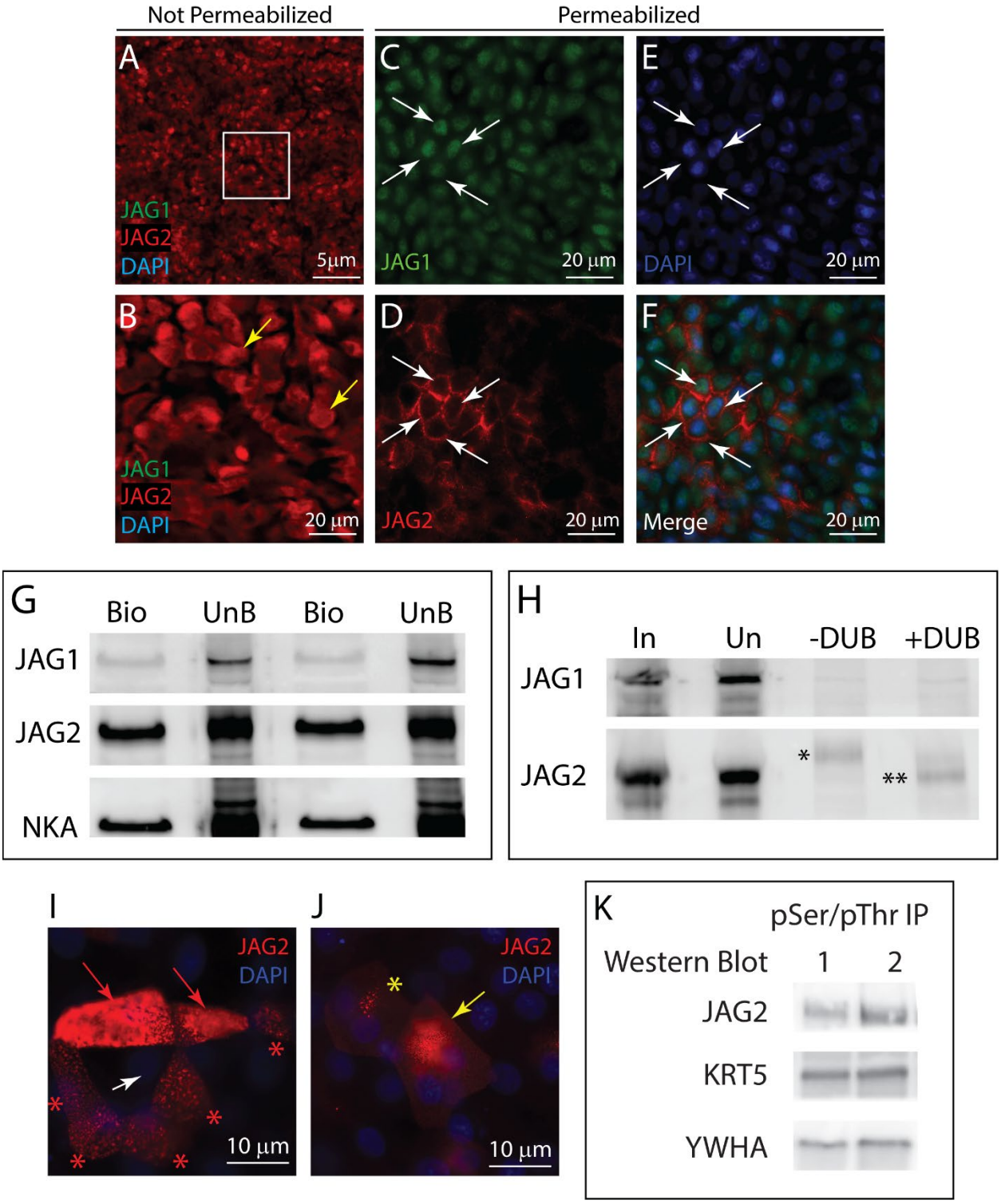
Not Permeabilized
Permeabilized
A
JAG1
JAG2
DAPI
5µm
C
JAG1
20 µm
E
DAPI
20 µm
B
JAG1
JAG2
DAPI
20 µm
D
JAG2
20 µm
F
Merge
20 µm
G
Bio
UnB
Bio
UnB
JAG1
JAG2
NKA
H
In
Un
-DUB
+DUB
JAG1
JAG2
*
**
I
JAG2
DAPI
10 µm
J
JAG2
DAPI
10 µm
K
pSer/pThr IP
Western Blot
1
2
JAG2
KRT5
YWHA

Figure 7

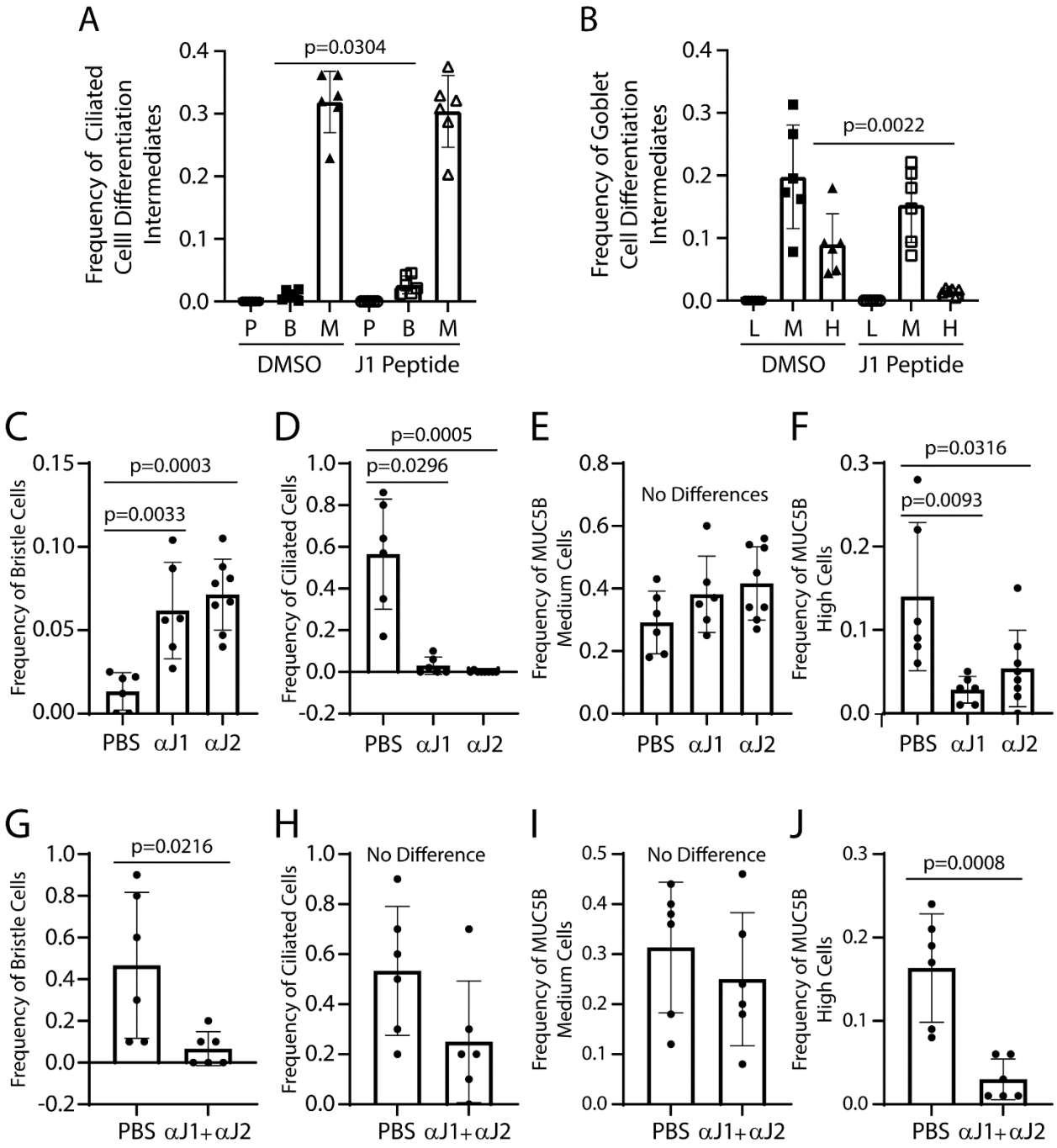
A
Frequency of Ciliated CellI Differentiation Intermediates
p=0.0304
P B M P B M
DMSO J1 Peptide
B
Frequency of Goblet Cell Differentiation Intermediates
p=0.0022
L M H L M H
DMSO J1 Peptide
C
Frequency of Bristle Cells
p=0.0003
p=0.0033
PBS αJ1 αJ2
D
Frequency of Ciliated Cells
p=0.0005
p=0.0296
PBS αJ1 αJ2
E
Frequency of MUC5B Medium Cells
No Differences
PBS αJ1 αJ2
F
Frequency of MUC5B High Cells
p=0.0316
p=0.0093
PBS αJ1 αJ2
G
Frequency of Bristle Cells
p=0.0216
PBS αJ1+αJ2
H
Frequency of Ciliated Cells
No Difference
PBS αJ1+αJ2
I
Frequency of MUC5B Medium Cells
No Difference
PBS αJ1+αJ2
J
Frequency of MUC5B High Cells
p=0.0008
PBS αJ1+αJ2

Supplemental Figure 1

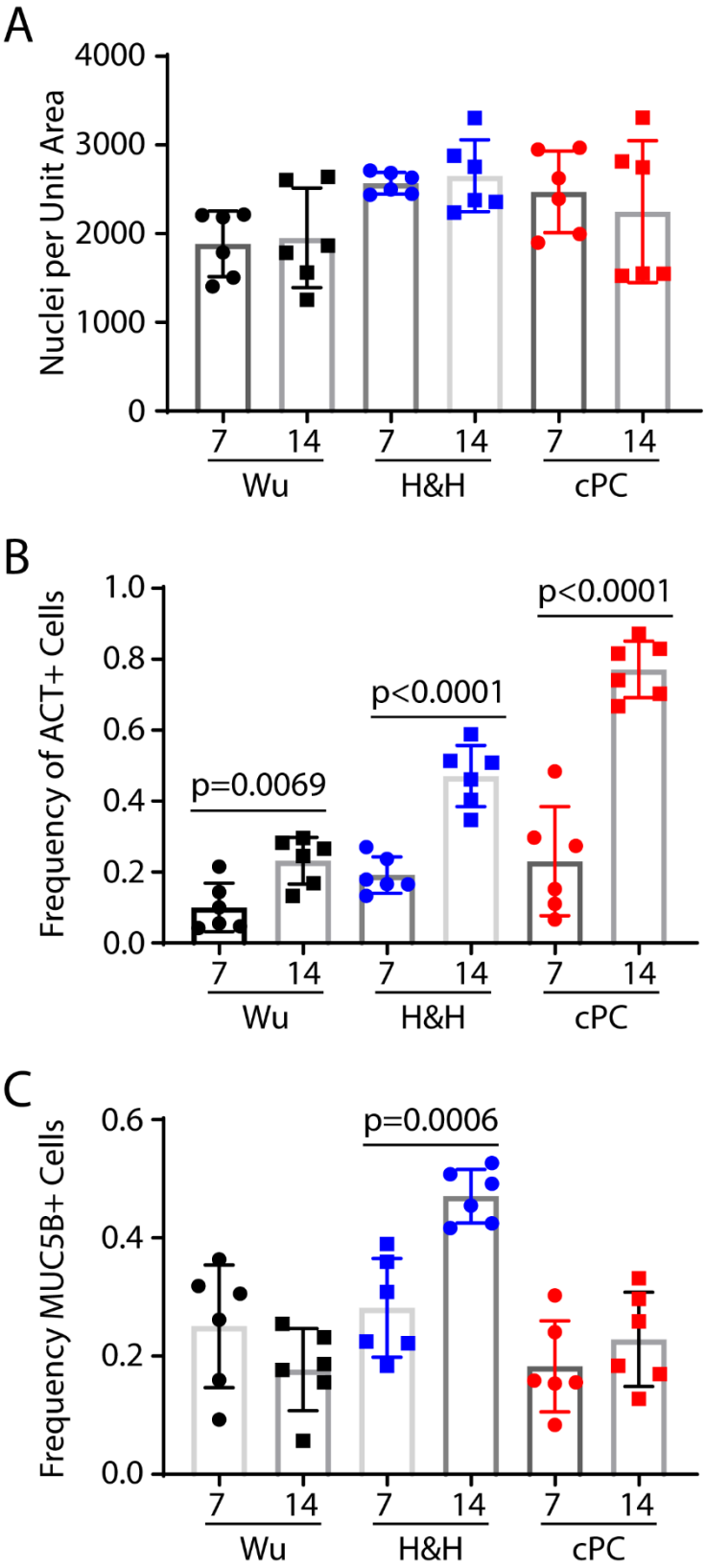

# Supplemental Figure 2

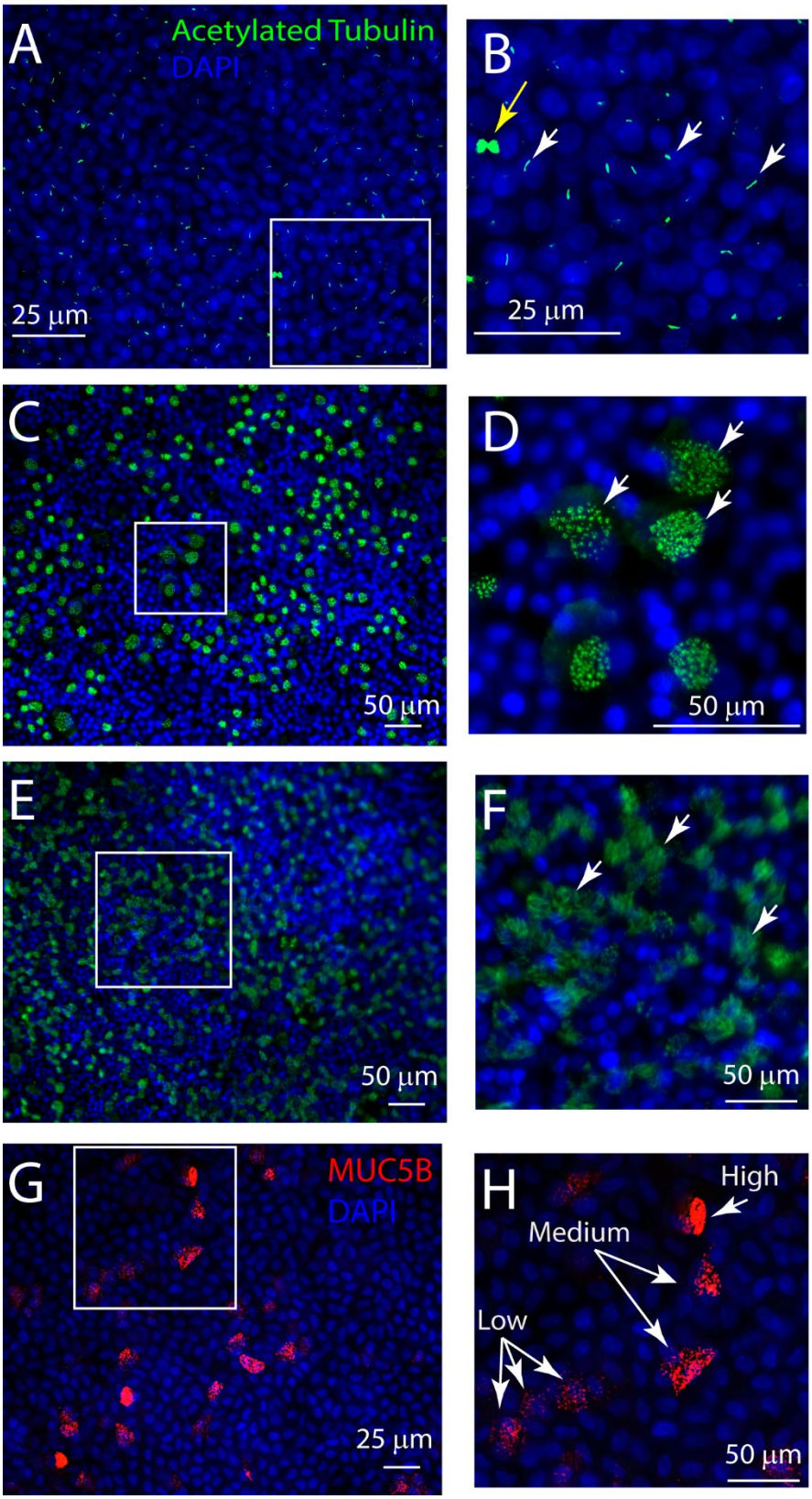

# Supplemental Figure 3

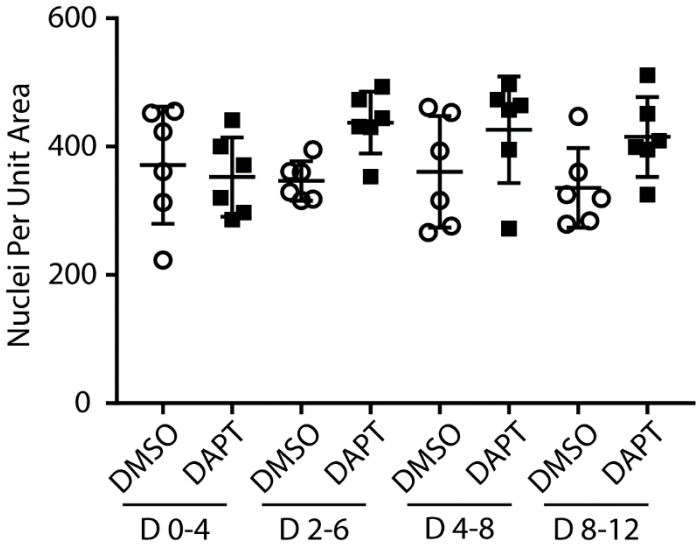

Supplemental Figure 4

Diferentiation Day 7

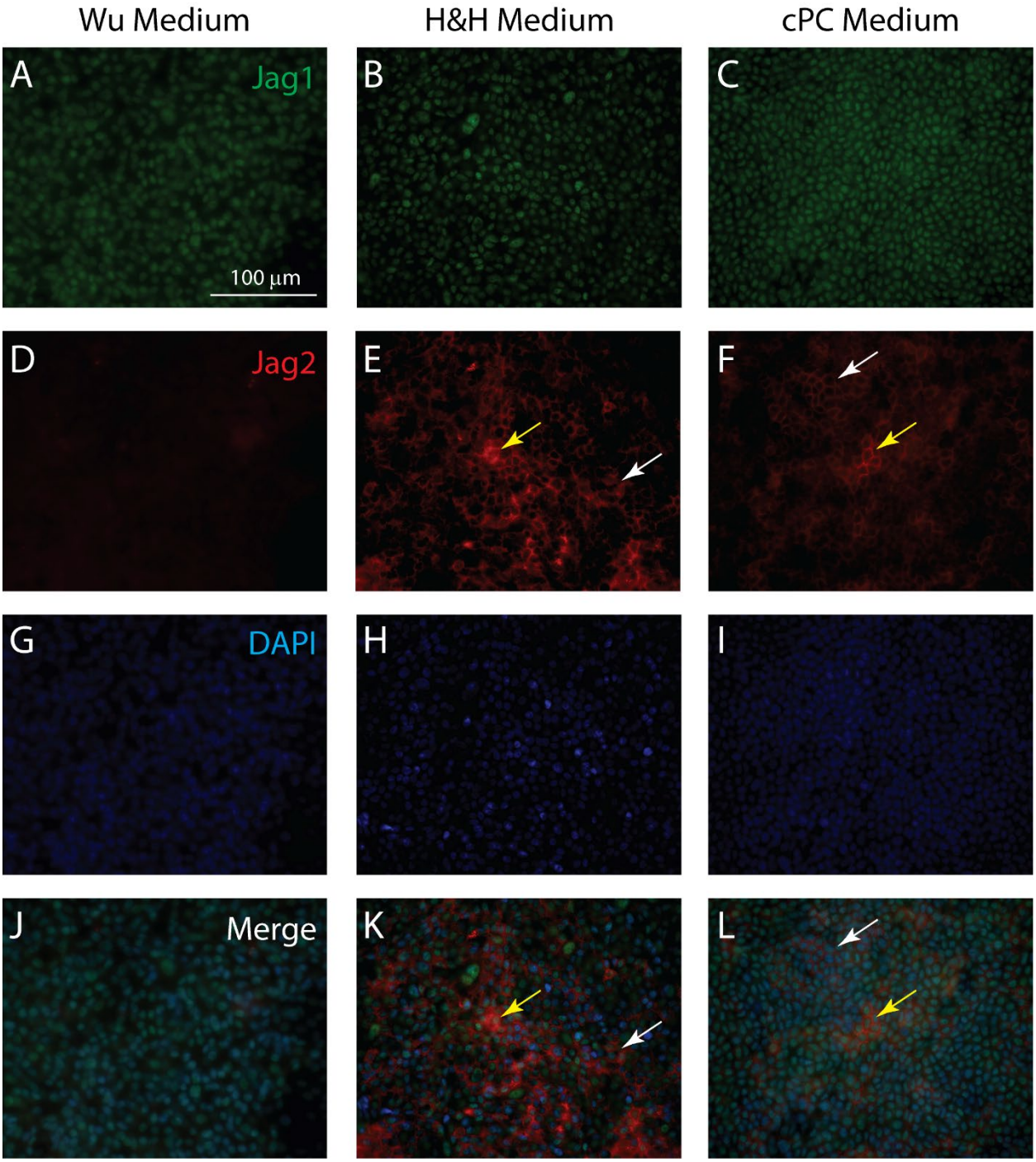

# Supplemental Figure 5

A

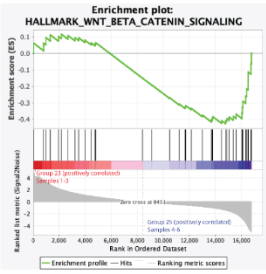


Enrichment Score = -0.427
FDR q-value = 0.0332
Leading Edge Genes = 14

C

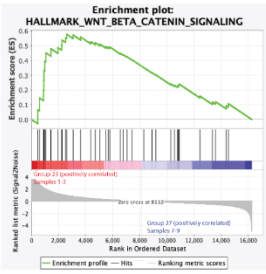


Enrichment Score = +0.578
FDR q-value = 0.0169
Leading Edge Genes = 13

E

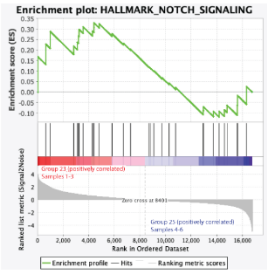


Enrichment Score = +0.368
FDR q-value = 0.506
Leading Edge Genes = 9

G

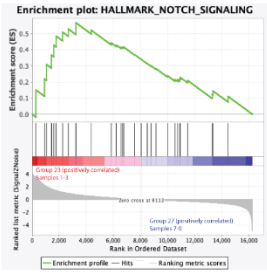


Enrichment Score = +0.567
FDR q-value = 0.0379
Leading Edge Genes = 10

B

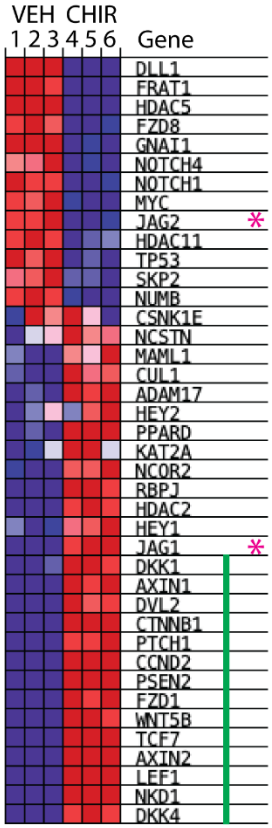


D

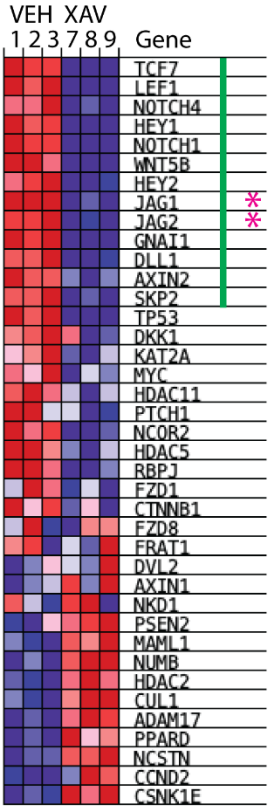


F

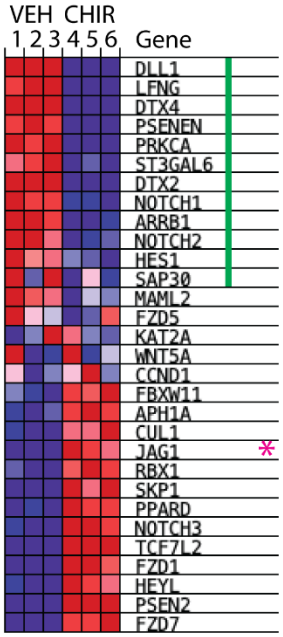


H

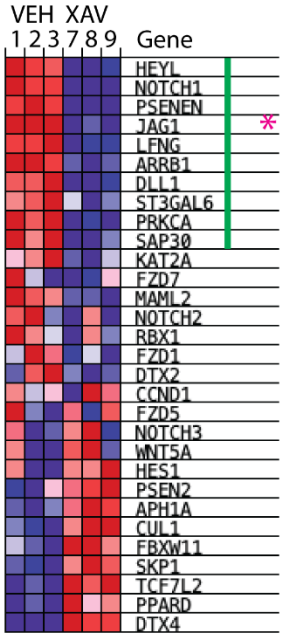


I

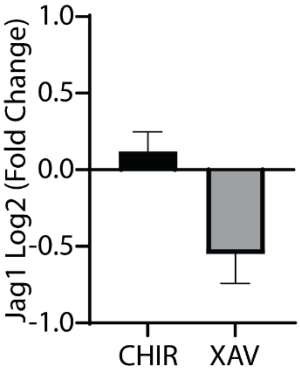


J

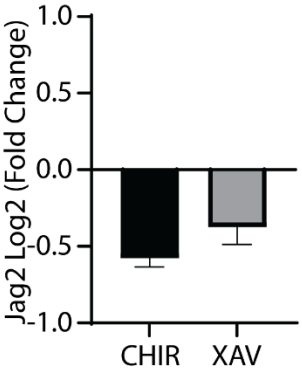

# Supplemental Figure 6

| Pathway | WNT | | NOTCH | | Target | | | |
|---|---|---|---|---|---|---|---|---|
| Treatment | CHIR | XAV | CHIR | XAV | bCat | GSK3 | TNKS | |
| ***Gene*** | | | | | | | | ***Full Gene Name*** |
| *Axin2* | | | | | Transc | (Protein) | Protein | *Axis Inhibition Protein 2* |
| *Lef1* | | | | | Transc | | | *Lymphoid Enhancer Binding Factor 1* |
| *Tcf7* | | | | | Transc | | | *Transcription Factor 7* |
| *Wnt5b* | | | | | | | | *Wnt Family Member 5B* |
| *Dll1* | | | | | Transc | | | *Delta Like Canonical Notch Ligand 1* |
| *Jag1* | | | | | Transc | | | *Jagged Canonical Notch Ligand 1* |
| *Notch1* | | | | | | Protein | Protein | *Notch Receptor 1* |
| *Lfng* | | | | | | | | *LFNG O-Fucosylpeptide 3-Beta-N-Acetylglucosaminyltransferase* |
| *Prkca* | | | | | | | | *Protein Kinase C Alpha* |
| *Psenen* | | | | | | | | *Presenilin Enhancer, Gamma-Secretase Subunit* |
| *Sap30* | | | | | | | | *Sin3A Associated Protein 30* |
| *St3gal6* | | | | | | | | *ST3 Beta-Galactoside Alpha-2,3-Sialyltransferase 6* |
| *Axin1* | | | | | | Protein | Protein | *Axis Inhibition Protein 1* |
| *Ccnd2* | | | | | | | | *Cyclin D2* |
| *Ctnnb1* | | | | | | | Protein | *Catenin Beta 1* |
| *Dkk1* | | | | | Transc | | | *Dickkopf WNT Signaling Pathway Inhibitor 1* |
| *Dkk4* | | | | | (Transc) | | | *Dickkopf WNT Signaling Pathway Inhibitor 4* |
| *Dvl2* | | | | | | | | *Dishevelled Segment Polarity Protein 2* |
| *Fdz1* | | | | | | | | *Frizzled Class Receptor 1* |
| *Nkd1* | | | | | | | (Protein) | *NKD Inhibitor Of WNT Signaling Pathway 1* |
| *Psen2* | | | | | | | | *Presenilin 2* |
| *Ptch1* | | | | | | | | *Patched 1* |
| *Gnai1* | | | | | | | | *G Protein Subunit Alpha I1* |
| *Hey1* | | | | | | | | *Hes Related Family BHLH Transcription Factor With YRPW Motif 1* |
| *Jag2* | | | | | | | | *Jagged Canonical Notch Ligand 2* |
| *Notch4* | | | | | | Protein | (Protein) | *Notch Receptor 4* |
| *Skp2* | | | | | | | | *Hes Related Family BHLH Transcription Factor With YRPW Motif 1* |
| *Ccdn1* | | | | | | | | *Cyclin D1* |
| *Dtx4* | | | | | | | | *Deltex E3 Ubiquitin Ligase 4* |
| *Maml2* | | | | | | | | *Mastermind Like Transcriptional Coactivator 2* |
| *Arrb1* | | | | | | | | *Arrestin Beta 1* |
| *Heyl* | | | | | | | | *Hes Related Family BHLH Transcription Factor With YRPW Motif Like* |

Upregulated in treated cells
Downregulated in treated cells
Transc: transcriptional
(Transc): based on similarity
(Protein): based on similarity
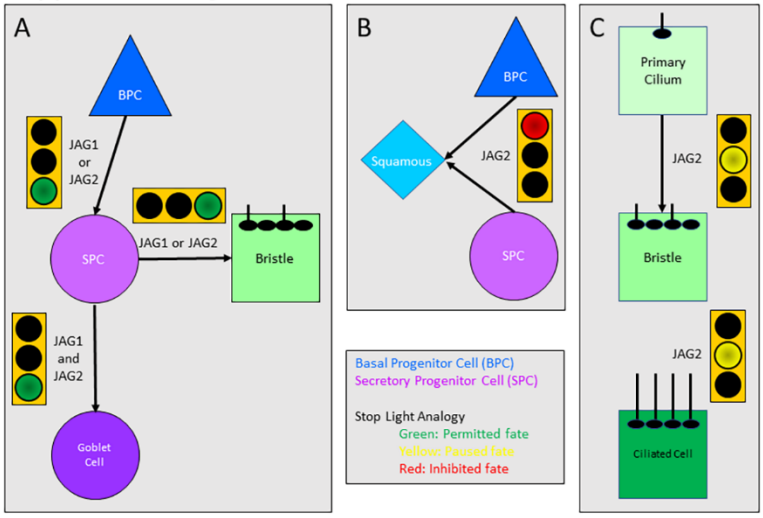
Supplemental Figure 7